EVALUATION OF MULTI-STAGE ACID FRACTURING TREATMENT IN DEEP CARBONATE FORMATION

A Thesis

by

WENYU ZHANG

Submitted to the Office of Graduate and Professional Studies of
Texas A&M University
in partial fulfillment of the requirements for the degree of

MASTER OF SCIENCE

Chair of Committee,	Ding Zhu
Committee Members,	Alfred Daniel Hill
	Yuefeng Sun
Head of Department,	Alfred Daniel Hill

December 2015

Major Subject: Petroleum Engineering

ABSTRACT

Acid fracturing techniques have been widely practiced to enhance well productivity and ultimate recovery for low permeability carbonate reservoirs. The success of an acid fracturing treatment is evaluated based on the productivity-index ratio. The evaluation of an acid fracturing treatment requires a comprehensive understanding of well completion methods, fracture propagation, acid fracture conductivity prediction, and post-treatment well performance analysis.

In this study, an integrated evaluation approach is developed to link all these processes in order to have a valid evaluation of a horizontal well multi-stage acid fracturing treatment. The model includes evaluation of the well completion methods, fracture propagation modeling, acid fracture modeling, and post-fractured well production prediction. A field treatment is evaluated in this study to illustrate the work procedure of this approach and its capability to handle field application.

From this study, it is concluded that one can apply the integrated approach developed from this research to evaluate an actual field multi-stage acid fracturing treatment, and help engineers to make better decisions.

DEDICATION

To my family

ACKNOWLEDGEMENTS

I would like to thank my advisors Dr. Zhu and Dr. Hill for their support and guidance during the course of my study. I also want to thank Dr. Sun for serving as my committee member. I am grateful for the help and support from my colleagues in Dr. Zhu and Dr. Hill's group.

I also would like to thank CNPC for the opportunity to work with a real field data. It was a valuable learning experience for me.

NOMENCLATURE

a	reservoir width
b	reservoir length
C	leak-off coefficient
C_A	acid concentration
C_D	dimensionless acid concentration
C_{fD}	dimensionless fracture conductivity
C_i	injected acid concentration
D_{eff}	effective diffusion coefficient
c_t	total compressibility
d_{pipe}	pipe diamter
d_{ball}	ball diameter
d_{perf}	perforation diameter
E	Young's Modulus
f_f	friction factor
f_{wall}	wall factor
g	gravitational acceleration
h_f	fracture height
J	productivity index
k	matrix permeability
k_f	fracture permeability
K'	flow consistency index
K_D	drag coefficient
K_d	discharge coefficient
K_I	stress intensity factor
$K_{I,G}$	stress intensity factor induced by modulus difference
$K_{I,\Delta P}$	stress intensity factor induced by net pressure
$K_{I,\ \Delta\rho h}$	stress intensity factor induced by gravity

$K_{I,\,\Delta\sigma}$	stress intensity factor induced by stress difference
L	tubing length
$m(p)$	pseudo-pressure
n'	flow behavior index
N_{perf}	open perforation number
N_{Re}	Reynolds number
p	pressure
p_i	initial formation pressure
p_{inj}	surface treating pressure / injection pressure
p_{net}	net pressure
p_p	formation pressure
$p_{res\text{-}face}$	bottomhole treating pressure
p_{wf}	bottomhole pressure
q	injection rate / production rate
q_D	dimensionless production rate
q_L	leak-off rate
r_e	external reservoir radius
r_w	wellbore radius
r'_w	effective wellbore radius
s	skin factor
s_f	fracture skin
s_R	partial penetration skin
t_{Dxf}, t_{Dye}	dimensionless time
v	velocity
v_{ball}	ball sealer velocity
v_{batch}	ball sealer batch velocity
V_L	leak-off volume
v_{slip}	slip velocity
V_{sp}	spurt loss volume

$v_{t,0}$	ball sealer terminal velocity
$v_{t,batch}$	ball sealer batch terminal velocity
w	fracture width
x_f	fracture half-length
y_e	distance of between fracture and reservoir boundary

Greek

α	Biot's constant
α_α	leak-off area propagation parameter
α_τ	fluid loss power coefficient
β	dissolving power
γ	specific gravity, dimensionless
Δp_{PE}	hydrostatic pressure drop
$\Delta p_{f,pipe}$	tubing friction
$\Delta p_{f,perf}$	perforation pressure drop
ε	roughness
θ	deviation angle
σ_c	formation closure stress
$\sigma_{h,min}$	minimum horizontal stress
σ_v	vertical stress
μ	viscosity
μ_{app}	apparent viscosity
ρ	density
ρ_{ball}	ball density, g/cm3
ρ_{fluid}	fluid density, g/cm3
ϕ	porosity, fraction
ϕ_{ball}	volume fraction of ball
τ	stress tensor / fluid loss delay time
υ	Poisson's ratio

TABLE OF CONTENTS

Page

LIST OF FIGURES

Page

LIST OF TABLES

Page

CHAPTER I

INTRODUCTION AND LITERATURE REVIEW

1.1 Research Background

Acid fracturing and proppant fracturing are two types of well stimulation methods. Both methods aim to create a conductive flow channel extending into the formation to increase contact area with the reservoir, and alter the flow pattern in the formation near the wellbore in order to enhance well production. In naturally fractured reservoirs, induced fractures can also create fracture network, which can significantly increase drainage volume of a well. Both stimulation methods have a long history in petroleum industry. Acid fracturing is more restricted to carbonate formation, while proppant fracturing can be performed in almost all types of formations. Even through acid fracturing and proppant fracturing share the same concept, due to the different mechanisms in creating fracture conductivity, design of acid fracturing treatment varies from proppant fracturing treatment.

Most carbonate formations are composed with calcite or dolomite, which are acid reactive minerals. Different from hydraulic fracturing treatments, which use proppant as conductivity agents, in acid fracturing treatments the fracture conductivity is created by the unevenly acid-etched fracture walls. A fracture is usually initiated by a pad fluid. Acid injection following the pad fluid into the fracture reacts with carbonate rock on the fracture walls. The heterogeneous characteristics of carbonate reservoirs lead to uneven etching of the fracture walls. As illustrated in **Fig. 1.1** (Kalfayan, 2007), when an acid fracturing

treatment is finished and the fracture closes, the parts that have less rock dissolved will act as pillars to keep the fracture open, and the parts that have more rock dissolved will leave conductive channels acting as path ways for hydrocarbon to flow towards wellbore.

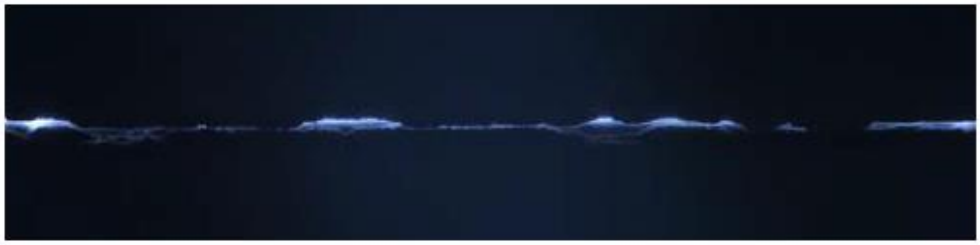

Figure 1.1 – Conductive channels created by acid-etched width from a carbonate sample (Kalfayan, 2007)

The application of multi-stage acid fracturing in horizontal wells is an alternative stimulation method to multi-stage proppant fracturing in tight carbonate reservoirs. With appropriate design, multi-stage acid fracturing can achieve similar results, but much more cost-effective, compares to proppant fracturing. Recent literatures (Etuhoko et al., 2014; Baumgarten and Bobrosky, 2009; Nainwal et al., 2006; Metcalf et al., 2007) prove that multi-stage acid fracturing application can be successful in tight carbonate formations.

The evaluation of acid fracturing is a complex procedure. The field operation may alter from the original treatment design. The results of an acid fracturing treatment are affected by many parameters. Post-treatment evaluation of created fracture geometry can be conducted by micro-seismic data, logging tool measurement, or pressure transient

analysis. These methods are all extremely uncertain. Another method to evaluate an acid fracturing operation is to use the productivity index ratio of after and before the treatment. The productivity index ratio measures the flow efficiency of a well. But it is a global measurement, and cannot identify the parameters that affect the stimulation results, such as effectiveness of the completion design or selected acid systems.

In this study, an integrated approach is developed to evaluate multi-stage acid fracturing treatments. The approach includes completion evaluation, fracture propagation simulation, acid fracture conductivity prediction, and post-fractured well productivity prediction. The ultimate goal is to evaluate field treatments more accurately and effectively.

1.2 Literature Review

The literature review covers four subjects; completion for multi-stage fracturing in horizontal wells, fracture propagation models, acid fracture models, and productivity models for fractured wells.

1.2.1 Development of multi-stage fracturing completion.

The development of horizontal drilling and advances in horizontal well completion have made it possible to effectively stimulate horizontal wells. One of these achievements is multi-stage fracturing technique which becomes a common stimulation method for low permeability formations. Based on isolation methods, the multi-stage fracturing technique can be divided into two groups; mechanical isolation, such as ball-activated sliding sleeve with open-hole packer, bridge plug, ball sealer; and chemical isolation; such as fiber or

foam. Sliding sleeve with open-hole pack completion and ball sealer completion will be reviewed in this study.

Sliding sleeve with open-hole packer is one of the most common techniques for multi-stage fracturing stimulation. It was first introduced in the early-2000s (Seale et al., 2006; Seale, 2007). It contains two main parts, a mechanical open-hole packer system capable of withstanding high differential pressures, and a series of fracturing ports, located between the packers that can be activated sequentially in one treatment as illustrated in **Fig. 1.2**. During a treatment, once all packers are set, and the wellbore is pressurized, a ball is dropped into the well that opens the last fracturing port at the toe of the well so that a fracture can be created at this location. Once the first fracture stage is finished, the second ball will be dropped into the well, the second ball isolate the first stage and open the second port for fracturing treatment.

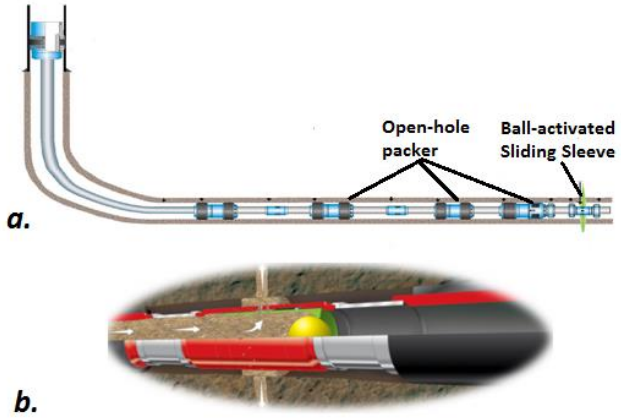

Figure 1.2 – a). Ball-activated sliding sleeves with open-hole packer completion (Seale et al., 2006) and b). sleeve activation (Tompkins et al., 2013)

The advantages of using ball-activated sliding sleeve are: high efficiency, no shutdown is required for multiple stage stimulation; well cleanup can be faster than plug and perf completion; can be performed in open-hole completion (Seale et al., 2006; Casero et al., 2013).

Ball sealer was first introduced in early 1956 and was proved to be a successful fluid diversion technique for multi-stage fracture treatments in cased and perforated vertical wellbores (Brown, 1963). Ball sealers are injected into a treated well for the purpose of contacting and sealing some perforations which are accepting the fluid flow as illustrated in **Fig. 1.3**. By blocking the entrance of some of the perforations, a new fracture can be created at the next perforation interval where the least fracturing resistance is found. The ball sealer technique was improved with development of buoyant ball sealer to overcome the low seating efficiency of conventional sink ball sealer (Erbstoesser, 1980).

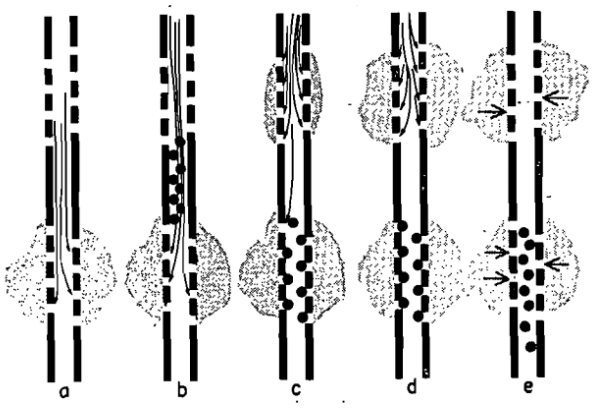

Figure 1.3 – Application of ball sealer for multi-stage stimulation (Neill et al., 1957)

Recently a combination using of perforation gun and ball sealers, named the Just-In-Time Perforating (JITP) technique, has been implemented in horizontal well multi-stage fracturing treatments (Angeles et al., 2012). As illustrated in **Fig. 1.4**, to operate a JITP treatment in a cased horizontal well, wireline gun assembly is first positioned at the first perforation set. After perforations are created, fluids are pumped to fracture the first stage. Then, ball sealers are dropped to block the first perforation set. After ball sealers sit on the perforations, the second stage stimulation can be performed. Repeat the process until all stages are complete.

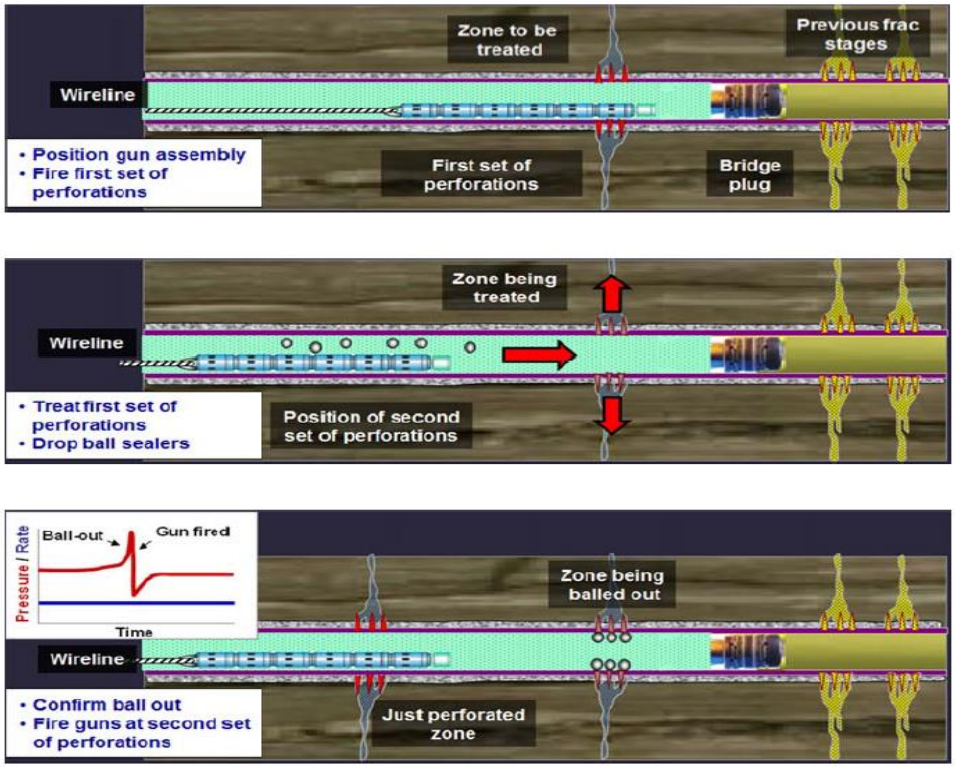

Figure 1.4 – Application of JITP for horizontal well multi-stage stimulation (Angeles et al., 2012)

The advantages of using ball sealers compared to ball-activated sliding sleeve are: balls are easier to flow back after treatment; production can start immediately after treatment, drill out of fracture port is not needed; can be performed in cased-hole completion; relatively cost-saving (Benish, 2013; Babaniyazov and Jackson, 2013).

Both ball-activated sliding sleeve in open-hole completion and ball sealers in cased and perforated well completion have their own advantages and disadvantages. No matter what completion method is selected for a multi-stage fracturing stimulation, the goal is to effectively isolate each fracture stage so when the main treatment begins, the fractures will be initiated within the designated intervals.

1.2.2 Development of fracture propagation models

The fracture propagation process in an acid fracturing stimulation is the same as for hydraulic fracturing. Hydraulic fracture modeling began in the late 1950s. Between the late 1950s and the early 1970s, numerous papers were published. Some early fundamental works include KGD (Zheltov and Khristianovitch, 1959; Geertsma and Klerk, 1969) and PK (Perkins and Kern, 1961) models. The PK model was further improved by adding fluid leakoff (Nordgren, 1972). The modified version is referred to as the PKN model.

Both KGD and PKN models are two-dimensional geomechanical models assuming a constant fracture height. Both models can predict fracture length and width growth with respect to injection. However, these two models approach the problem with different solutions. The KGD model, as shown in **Fig. 1.5**, is based on the assumption of horizontal plane strain condition, indicating that rock toughness is only considered in the horizontal plane. Fracture width, as a result, is independent of fracture height and is

constant in the vertical direction. A constant injection rate and approximately constant pressure in the fracture except for the fracture tip are also assumed to simplify the analytical solution. These assumptions yield a fracture model that has relative larger vertical extension than the horizontal extension.

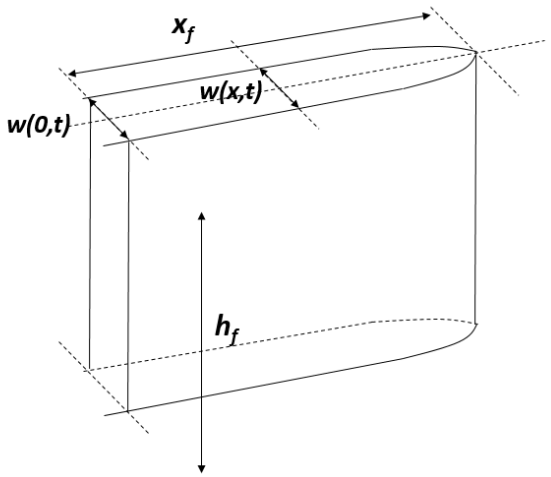

Figure 1.5 – The KGD fracture model

On the contrary, the PKN model, as shown in **Fig. 1.6**, is based on the assumption of vertical plan strain condition, indicating that rock toughness prevails in the vertical plane. The deformation of each vertical cross section of the fracture is independent. As a result, the cross sections obtain fracture width with an elliptical shape with maximum width in the center. Pressure in the fracture decreases towards the fracture tip. These

assumptions yield a fracture model that has a larger horizontal extension than vertical extension.

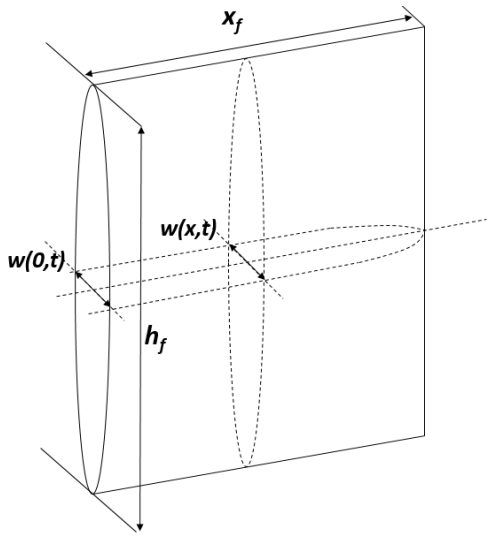

Figure 1.6 – The PKN fracture model

Based on previous work, more advanced fracture models that can calculate the fracture height variation with time at different fracture lengths were developed and named pseudo-3D fracture models. The early pseudo-3D fracture models (Settari and Cleary, 1986; Morales and Sayad, 1989) evolved from the PKN model followed the same assumptions such as predominantly 1D horizontal fluid flow and the vertical plane strain condition. The approach for fracture height calculation varies in different pseudo-3D models. Palmer and Carroll (1983) proposed a numerical solution for fracture height growth in multilayered, asymmetrical formations based on the work presented by

Simonson et al. (1978). It determines the fracture height from the local net pressure, stress profile, and rock toughness by satisfying the static equilibrium of the fracture. This concept is adopted in many pseudo-3D models.

In order to improve the performance of pseudo-3D models, especially when large stress barriers are not present, modeling vertical flow in the fracture is necessary. The modified pseudo-3D models (Meyer, 1989; Weng, 1992) that incorporate 2D fluid flow not only retain their ability to handle complicated layered stress, modulus, toughness, and leak-off, but also improve the performance on fracture height containment.

Instead of planar fracture, the fracture geometry can be much more complex because of heterogeneous formation stress field and the presence of pre-existing natural fractures. Fully 3D fracture models that can simulate both fracture dimensions growth and fracture orientation changes during a fracturing process have been developed. However, such complicated models require extensive computational time.

Considering computational efficiency and model accuracy, a pseudo-3D fracture propagation model is selected for this study. The details of this model are presented in Chapter II.

1.2.3 Development of acid transport and reaction models and acid fracture conductivity correlations

For acid fracturing, fracture conductivity is essentially calculated from acid-etched width. Once a fracture is created by pad fluid, the acid transport and reaction model during acid injection are used to generate acid concentration profile in the fracture and estimate

the acid-etched width. From fracture conductivity correlations, the final fracture conductivity for an acid fracturing treatment can be obtained.

In early acid fracture models (Lo and Dean, 1989; Settari, 1993), the fluid flow was assumed only in one dimension with vertical fluid fronts. Acid diffusion from the center of a fracture to the fracture walls is calculated based on empirical formulations that assume a constant fracture width, infinite reaction rate, and no entrance effects. Romero et al. (2001) developed an implicit 3D acid fracturing simulator that involves two-dimensional fluid transport, along the fracture length and height, and acid diffusion calculation across the fracture width. When calculating acid diffusion across the width, finite difference mesh was constructed, so that acid concentration can be tracked at each grid block. The simulator is also coupled with acid reaction and fracture-height growth formulas. However, the finite difference grid block used in Romero's simulator can only handle grid block with dimensions of several feet to tens of feet, which is too large to capture local formation heterogeneity (Mou et al., 2009). A more advanced 3D acid fracturing simulator was developed by Oeth et al. (2013). Compares to Romero's model, much smaller grid dimensions, on magnitude of inches, are used in order to capture the local formation heterogeneity. The fluid velocity field is obtained by solving Navier-Stokes equations in a fracture domain using Semi-Implicit Method for Pressure-Linked Equations (SIMPLE). Front-fixing methods is used to handle the irregular fracture boundaries, which evolves with time due to rock dissolution. In this way, the fluid velocity and pressure fields in the fracture can be fully modeled in three dimensions.

Another important part in acid fracture modeling is the estimation of acid fracture conductivity, which is strongly related to acid-etched width. Nierode and Kruk (1973) introduced an empirical correlation between acid-etched width and fracture conductivity based on the results of 25 experiments. It is concluded from their laboratory work that the acid-fracture conductivity can be presented as,

$$wk_f = C_1 \exp\left(-C_2 \sigma_c\right) \tag{1.1}$$

where C_1 is a constant related to amount of dissolved rock, C_2 is a constant related to rock embedment strength, and σ_c is formation the closure stress. However, as Nierode and Kruk (1973) stated in their paper, the correlation drawn from the experimental results may not be able to represent the heterogeneity effect of the carbonate core samples, and it may only provide a lower bound on the fracture conductivity attained in the field. Several more acid-fracture conductivity correlations (Ming et al., 1999; Nieto et al., 2008) were developed mostly based on experimental results. Deng et al. (2011) developed a new correlation that accounts for permeability and mineralogy distributions, and rock elastic properties on overall acid fracture conductivity, based on numerical experiments. The new correlation introduces three geostatistic parameters, the dimensionless horizontal and vertical correlation lengths, and normalized standard deviation of the natural logarithm of permeability. The former two parameters describe how continuous permeability is distributed along the horizontal or vertical direction. The normalized standard deviation represent the permeability variation from the average value.

In this study, an in-house acid fracturing simulator (Oeth, 2013), which is based on the acid transport and dissolution models developed by Mou et al (2007, 2009). and the

acid fracture conductivity correlation developed by Deng et al. (2011), is selected to simulate the fracture conductivity change during the acid injection process. The details of this simulator are presented in Chapter II.

1.2.4 Development of fractured-well productivity models

The models for predicting fractured-well productivity are usually based on idealized flow regimes including bilinear flow, linear flow, and pseudo-radial flow. Prats (1961) developed a simple analytical model for determining vertically fractured well productivity. The productivity-index ratio is expressed as,

$$\frac{J}{J_o} = \frac{\ln\left(\frac{r_e}{r_w}\right)}{\ln\left(\frac{r_e}{r'_w}\right)} \tag{1.2}$$

where, J is the fractured well productivity, J_o is the original well productivity, r_e is reservoir drainage radius, r_w is wellbore radius, r'_w is the effective wellbore radius which is one half of fracture half-length $x_f/2$. In the Prats' model, it is assumed that the flow is under steady-state condition, reservoir has a cylindrical drainage area, reservoir fluids are incompressible, and fracture height is equal to formation thickness. Based on Prats' model, Meyer and Jacot (2005) found an analytical solution for predicting the productivity of a well with a finite-conductivity vertical fracture under pseudosteady-state condition. In their model, the effective wellbore radius is related to both dimensionless fracture conductivity and fracture half-length instead of only fracture half-length in Prats' model. The new effective wellbore radius is defined as,

$$r_w^{'} = \frac{x_f}{\frac{\pi}{C_{fD}} + 2} \tag{1.3}$$

where C_{fD} is the dimensionless fracture conductivity, which is defined by,

$$C_{fD} = \frac{k_f w}{k x_f} \tag{1.4}$$

where k_f is the fracture permeability, w is the fracture width, and k is the matrix permeability. With the new effective wellbore radius, the fracture skin can be calculated as,

$$s_f = \ln\left(\frac{r_w}{r_w^{'}}\right) \tag{1.5}$$

By substituting skin factor with fracture skin in well deliverability equations, one can calculate the production rate of a fractured well.

However, it is noticed that in low permeability formations, such as tight gas formations or shale formations, the time to reach pseudosteady-state condition may take years. Several papers (Barker and Ramey, 1978; Cinco-Ley and Samaniego-V, 1981) have been published on determining production for a vertically fractured well with transient flow condition. Wattenbarger et al. (1998) presented a solution for production analysis of tight gas wells with infinite-conductivity fractures. In their model, both production predictions for early time (transient period) and late time (depletion period) can be calculated. The model assume that the fracture has an infinite conductivity, which is a good assumption for dimensionless fracture conductivity larger than 50. The model also assumes linear flow in a rectangular reservoir.

Prediction of the productivity of a horizontal well intersects with multiple transverse fractures can be done by dividing the total well drainage area into individual fracture blocks. Each block represents the drainage volume of a fracture. Then, productivity models of a vertically-fractured well can be applied to each fracture. The total productivity of the stimulated horizontal well is the sum of productivity from every fracture block (Song et al., 2011). This method is valid when the permeability of the formation is low and interactions between fractures can be neglected.

In this study, production forecast is conducted using the linear flow model for the fractured wells developed by Wattenbarger et al. (1998). The details of the solution of this model are presented in Chapter II.

1.3 Research Objectives

Through the literature review, it is clear that the evaluation of a multi-stage acid fracturing treatment is an integrated process. Due to the complexity of multi-stage completion and the mechanisms associated with reaction of acid with a heterogeneous carbonate rock, the performance of a multi-stage acid fracturing treatment in a horizontal well is difficult to forecast. The key to accurately predict the short-term and long-term production or productivity-index ratio of a post-fractured horizontal well is to have a comprehensive understanding of the treatment design and the formation. The ultimate goal for this research is provide a model that can be used as a guideline for evaluating a complex multi-stage acid fracturing treatment for a horizontal well. The detailed objectives for this this research are as the following:

1. Develop an integrate evaluation model for a multi-stage acid fracturing treatment. The model will combine completion evaluation, fracture propagation simulation, acid fracture conductivity simulation, and post-treatment well performance prediction into a continuous procedure.
2. Develop an evaluation procedure for a field application based on the specific treatment design use the approach.
3. Demonstrate the evaluation process of the field treatment using the integrated approach.

CHAPTER II

THEORETICAL APPROACH

To evaluate the performance of a multi-stage acid fracturing treatment of a horizontal well, it is important to know the geometry and conductivity of the fractures. Based on well completion design, the number and location of treated intervals on a well can be determined. From treatment design and operational records, fracture dimensions and conductivity can be modeled through fracture simulators. With known fracture and reservoir properties, the total well productivity of a horizontal well with multi-stage fractures can be predicted.

In this chapter, the evaluation of completions for multiple stage fracturing used in this study is presented. These evaluations are based on pressure analysis of treatment injection records. From the pressure records during injection of a treatment, ball-sitting efficiency, sleeve opening and frictional pressure drop can be diagnosed. The details of a pseudo-3D fracture propagation model, a 3D acid fracture model, and a post-fractured well productivity model that are used in this study are also presented in this Chapter. Finally, the approach of integrating those elements into a comprehensive treatment evaluation model is demonstrated.

2.1 Evaluation of Horizontal Well Multi-stage Fracturing Completion

When select completion methods for multi-stage acid fracturing of a horizontal well, it is important to know how completions are designed to execute fracturing. The functions of completion in such a case include isolation between stages, establish a

pathway for fluid to enter the formation, and generate enough velocity/pressure difference to initialize fracture. In this section, the mechanisms of ball-activated sliding sleeve with open-hole packer, ball sealer, and pressure-controlled sliding sleeve are demonstrated. Prediction of job-friction during a treatment is also discussed.

2.1.1 Ball-activated sliding sleeve with open-hole packer

Ball-activated sliding sleeve is a mechanical stage isolation device. Compared to plug and perf completion, the operation time is much shorter. As illustrated in **Fig. 1.2,** it contains two main parts, a mechanical open-hole packer system that is capable of withstanding high differential pressures, and a series of fracturing ports. Each fracturing port have a ball seat, and size of ball seats increases from the first stage to the last stage. Once the sleeve is pushed open by a ball seating on the ball seat, the treating fluids can enter the annulus between tubing and formation through the perforations on the tubing. The operation using ball-activated sliding sleeve and open-hole packer follows these steps:

1. Run production casing or liner and downhole assembly into the well
2. Before the main treatment, a ball is dropped with treating fluid. When the ball lands on the specific ball seat, back pressure in the tubing increases. When the pressure exceeds the maximum pressure that the sliding sleeve can hold, the sleeve is pushed open. Usually, the opening of a fracturing sleeve will cause a pressure spike showing on the surface treating pressure as illustrated in **Fig. 2.1**, indicating the first stage is ready to be pumped.
3. Following this indication, the main treatment can be started by pumping the treatment fluids for the first stage.

4. When the first stage is finished, land the next ball to initiate the second treatment stage.
5. Repeat until all stages are complete.
6. Flow back the well to collect the balls, or mill the fracturing port for production.

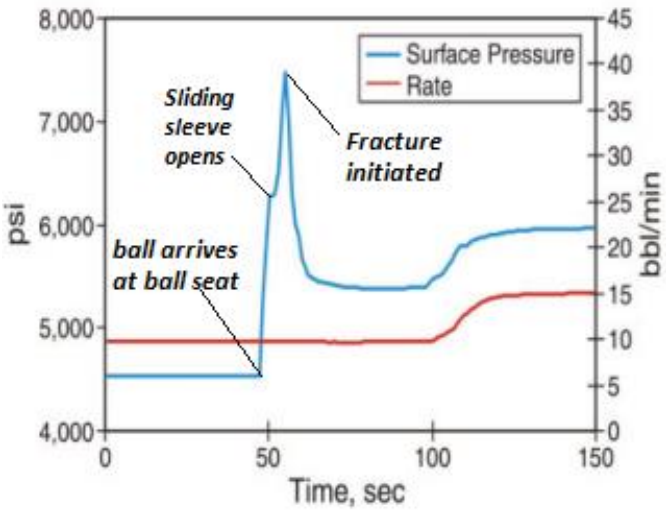

Figure 2.1 – An example of pressure response when ball arrives ball seat, sleeve opens, and fracture initiated (Augustine, 2011)

Fig. 2.1 is a useful tool for completion diagnosis. If the balls work correctly, and fractures are initiated accordingly, the pressure record should show a sudden increase when the ball is set on the ball seat, a small pressure drop when the sleeve opens, and a sudden pressure drop when the fracture is initiated.

2.1.2 Ball sealers

Another mechanical isolation method in multi-stage stimulation is the use of ball sealers. Different from ball-activated sleeves, ball sealers are usually used in cased and perforated wells. When pumped into an injection well, balls will be carried to open perforations by injection fluid, and will sit on the perforations to block the fluid enters the perforations. The successful use of ball sealers depends on many factors, and the analysis is much more complicated compared to ball-activated sleeves. In order to understand the behavior of ball sealers, numerous studies and experiments have been conducted on determining ball terminal velocity and ball seating efficiency.

Knowing the velocity of ball sealers can provide the time ball sealers arrive at perforation intervals. By monitoring the pressure behavior after the ball sealers arrive at the perforation intervals, the activation of the corresponding stage or the initiation of the fracture at that perforation set can be diagnosed. It helps engineers to schedule the treatment fluids accordingly. A common assumption in calculating ball sealer velocity is that the particles do not disturb the velocity of the fluid (Li et al., 2005). The velocity of a ball sealer, v_{ball}, can be defined by,

$$v_{ball} = \frac{q}{A_{pipe}} + v_{slip} \approx \frac{q}{A_{pipe}} + v_{t,0} \tag{2.1}$$

where $v_{t,0}$ is the terminal settling or rising velocity for a single spherical particle in ft/min, and is defined by (Nozaki et al. 2013),

$$v_{t,0} = 20\frac{\rho_{ball} - \rho_{fluid}}{\left|\rho_{ball} - \rho_{fluid}\right|} f_{wall}\sqrt{\frac{g d_{ball}\left|\rho_{ball} - \rho_{fluid}\right|\cos\theta}{\rho_{fluid} K_D}} \tag{2.2}$$

where ρ_{ball} and ρ_{fluid} are densities of ball sealer and carrying fluid in g/cm^3, K_D is the drag coefficient, θ is deviation angle in degrees, g is the acceleration of gravitation in ft/s^2, and f_{wall} is wall factor which estimates the interaction between ball sealer and tubing wall.

The drag coefficient and the wall factor is a function Reynolds number. For a Newtonian fluid, the Reynolds number is defined as,

$$N_{\mathrm{Re}} = \frac{129\left|v_{slip}\right| d_{ball}\rho_{fluid}}{\mu} \tag{2.3}$$

Based on the calculated Reynolds number, the drag coefficient K_D can be determined by Eq. 2.4 – Eq. 2.6 (Gabriel and Erbstoesser, 1984). When $N_{Re} < 0.1$,

$$K_D = \frac{24}{N_{\mathrm{Re}}} \tag{2.4}$$

when $0.1 < N_{Re} < 1000$,

$$K_D = \left(\frac{24}{N_{\mathrm{Re}}}\right)\left(1 + 0.14 N_{\mathrm{Re}}^{0.7}\right) \tag{2.5}$$

when $1000 < N_{Re} < 35000$,

$$K_D \cong 0.445 \tag{2.6}$$

The wall factor in different Reynolds number regime can be determined by Eq. 2.7 – Eq. 2.9 (Chhabra et al., 2003). When $N_{Re} < 1$,

$$f_{wall} = \frac{1 - 2.105\left(\frac{d_{ball}}{d_{pipe}}\right) + 2.0865\left(\frac{d_{ball}}{d_{pipe}}\right)^3 - 1.7065\left(\frac{d_{ball}}{d_{pipe}}\right)^5}{1 - 0.75857\left(\frac{d_{ball}}{d_{pipe}}\right)^5} + \frac{0.72603\left(\frac{d_{ball}}{d_{pipe}}\right)^6}{1 - 0.75857\left(\frac{d_{ball}}{d_{pipe}}\right)^5} \tag{2.7}$$

when $1 < N_{Re} < 200$,

$$f_{wall} = \left(\frac{1 - \frac{d_{ball}}{d_{pipe}}}{1 - 0.33\frac{d_{ball}}{d_{pipe}}}\right)^{\frac{3.3 + 0.0085N_{Re}}{1 + 0.1N_{Re}}} \tag{2.8}$$

when $200 < N_{Re}$,

$$f_{wall} = \left[1 - \left(\frac{d_{ball}}{d_{pipe}}\right)^2\right]\left[1 - \frac{1}{2}\left(\frac{d_{ball}}{d_{pipe}}\right)^2\right]^{0.5} \tag{2.9}$$

When the density of the ball sealer is the same as that of the carrying fluid, the terminal settling velocity of the ball sealer is zero. However, if the densities of the ball sealer and the carrying fluid are not the same, iterations for calculating of the terminal velocity of the ball sealer needs to be performed. First, a terminal velocity for ball sealer is assumed, use this assumed velocity to calculate Reynolds number. Sequentially, both drag coefficient and wall factor can be determined. Input drag coefficient and wall factor into Eq. 2.2 to calculate new terminal velocity of the ball sealer. If the new velocity varies

largely from the assumed value, it is necessary to use the new velocity to calculate new drag coefficient and wall factor. Repeat the iteration until the difference between the new terminal velocity and the previous one is acceptable.

For example, in a vertical well with wellbore diameter of 0.25 ft, ρ_{ball} is 1.1 g/cc and ρ_{ball} is 1.0 g/cc, and the ball diameter is 0.5 inches. Assume initial ball sealer terminal velocity as 0.2 ft/min, form Eq. 2.3, the Reynolds number is calcualted,

$$N_{\mathrm{Re}} = \frac{129\left|v_{slip}\right| d_{ball}\rho_{fluid}}{\mu} = \frac{129\times 0.2\times 0.5/12\times 62.4}{30} = 2.236 \tag{2.10}$$

the drag coefficient and wall factor can be determined by Eq. 2.5 and Eq. 2.8,

$$K_D = \left(\frac{24}{2.236}\right)\times\left(1+0.14\times 2.236^{0.7}\right) = 31.09 \tag{2.11}$$

$$f_{wall} = \left(\frac{1-\dfrac{0.5/12}{0.25}}{1-0.33\dfrac{0.5/12}{0.25}}\right)^{\frac{3.3+0.0085\times 2.236}{1+0.1\times 2.236}} = 0.934 \tag{2.12}$$

substitute the drag coefficient and wall effect and other parameters into Eq. 2.2, the new terminal velocity can be calculated as,

$$v_{t,0} = 20\times\frac{1.1-1.0}{\left|1.1-1.0\right|}\times 0.934\times\sqrt{\frac{32.174\times 0.5/12\times\left|1.1-1.0\right|\times\cos 0^{\circ}}{1.0\times 31.09}} \tag{2.13}$$
$$= 0.9\ ft/\min$$

Since the error between calculated and assumed ball sealer terminal velocity is very large, we need to perform the calculation again with the new velocity. Starting from Reynolds number,

$$N_{\mathrm{Re}} = \frac{129|v_{slip}|d_{ball}\rho_{fluid}}{\mu} = \frac{129\times 0.9\times 0.5/12\times 62.4}{30} = 10.44 \tag{2.14}$$

new drag coefficient and wall factor can be determined,

$$K_D = \left(\frac{24}{10.44}\right)\times\left(1+0.14\times 10.44^{0.7}\right) = 14.49 \tag{2.15}$$

$$f_{wall} = \left(\frac{1-\frac{0.5/12}{0.25}}{1-0.33\frac{0.5/12}{0.25}}\right)^{\frac{3.3+0.0085\times 10.44}{1+0.1\times 10.44}} = 0.811 \tag{2.16}$$

substitute the drag coefficient and wall effect and other parameters into Eq. 2.2, the new terminal velocity can be calculated as,

$$v_{t,0} = 20\times\frac{1.1-1.0}{|1.1-1.0|}\times 0.811\times\sqrt{\frac{32.174\times 0.5/12\times|1.1-1.0|\times\cos 0^{\circ}}{1.0\times 14.49}} \tag{2.17}$$
$$= 1.56\ ft/\min$$

Repeat the procedure and we can obtain the final ball sealer terminal velocity of 1.94 ft/min, with error between two iterations less than 0.05%.

In some cases, ball sealers are dropped in form of batches. For this type of injection, hydrostatic effect, the momentum transfer hindrance, and the wall effect need to be considered. The average terminal velocity for ball sealer batch, v_{batch} , is defined by (Barnea and Mizrahi, 1973),

$$v_{batch} = \frac{\phi_{ball}}{1-\phi_{ball}}\frac{q}{A_{pipe}} + \phi_{ball}v_{t,batch} \tag{2.18}$$

Where ϕ_{ball} is the volume fraction occupied by the ball sealers, $v_{t,batch}$, is the terminal velocity for ball-sealer batch defined by,

$$v_{t,batch} = \frac{1-\phi_{ball}}{\left(1+\phi_{ball}^{1/3}\right)\exp\left[\frac{5\phi_{ball}}{3(1-\phi_{ball})}\right]} v_{t,0} \tag{2.19}$$

where $v_{t,0}$ can be calculated using Eq. 2.2.

Erbstoesser (1980) and Bern and Lewis (1992) conducted experimental work on ball sealer seating efficiency with respect to different pump rates, ball densities, and pipe deviation angles, the results are shown in **Fig. 2.2**. In **Fig. 2.2**, picture (a) shows the test results for a vertical pipe; picture (b) shows the test results for a 60˚ deviated pipe; picture (c) shows the test results for a 75˚ deviated pipe; and picture (d) shows the test results for a horizontal pipe. From the test results, the ball seating efficiency for the horizontal pipe remained lower than 50% regardless of the ball density or pump rate. This indicates that ball sealer is not an ideal method for isolation in horizontal wells or highly deviated wells.

From the pressure record during a fracture treatment, if the balls are sit as designed, pressure should increase until formation breakdown and fracture is initiated. This can help to diagnose ball sealer's efficiency.

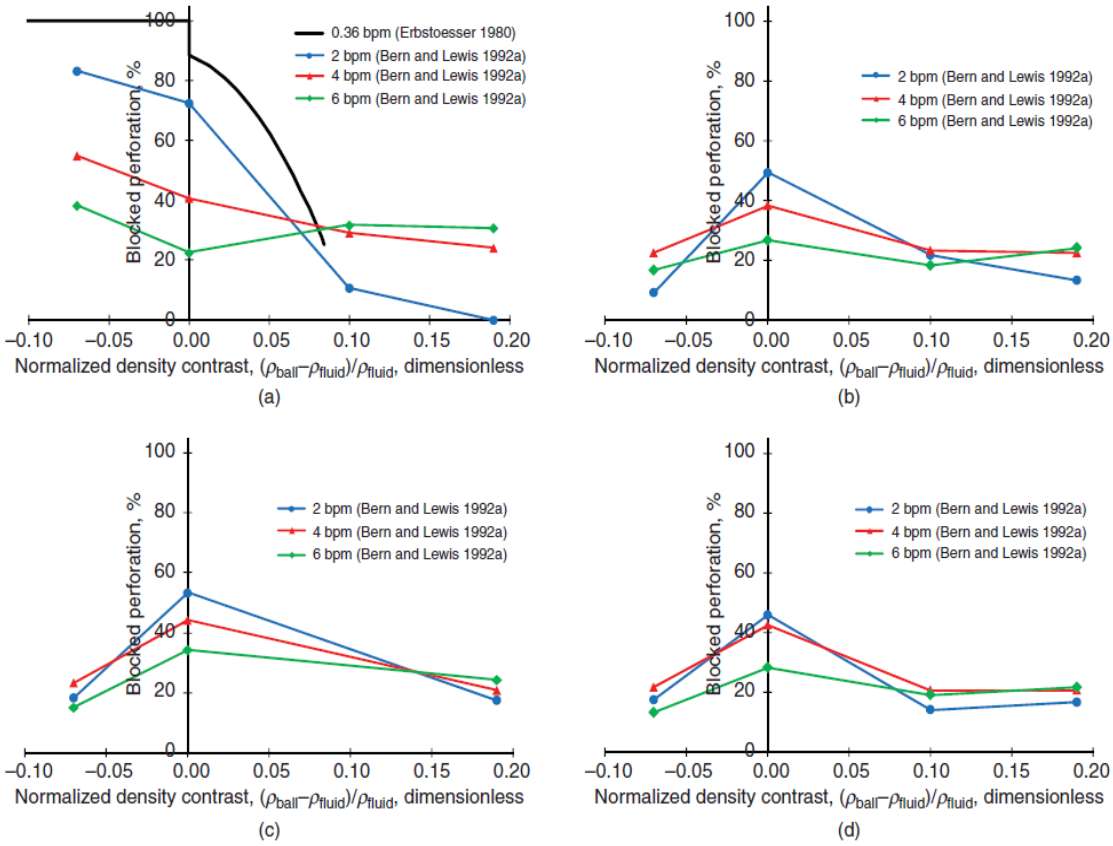

Figure 2.2 – Blocked perforation percentage vs. normalized density contrast (Nozaki et al., 2013)

2.1.3 Pressure-controlled sliding sleeve with open-hole packer

Downhole isolation for stage stimulation can also be achieved by Pressure-controlled sliding sleeve with open-hole packer. The isolation mechanism of this completion is a combination of ball-activated sliding sleeve and ball sealer designs. **Fig. 2.3** illustrates the procedure of a multiple stage treatment using this completion. In this type of completion, a series of pressure-controlled sleeves and open-hole packers will be sent downhole with the liner assembly. The pressure required to open each pressure-

controlled sleeve is designed with a specific value. The opening pressures for all pressure-controlled sleeves should be above the maximum possible bottomhole flowing pressure during the treatment, so that the sleeves will not accidentally open when the treatment is carried out. Also the pressures should increase from toe to heel, so that engineers can control the stage isolation and fluid placement for each treating interval. The first stage treatment is usually executed using a ball-activated sliding sleeve. After the first stage fracturing is complete, ball sealers are used to plug perforations on the opening sleeve until the pressure build up to a certain value to push the next sleeve open. Once the treatment for stage 2 is completed, more ball sealers are dropped. Repeat the process until multiple stage treatments are finished.

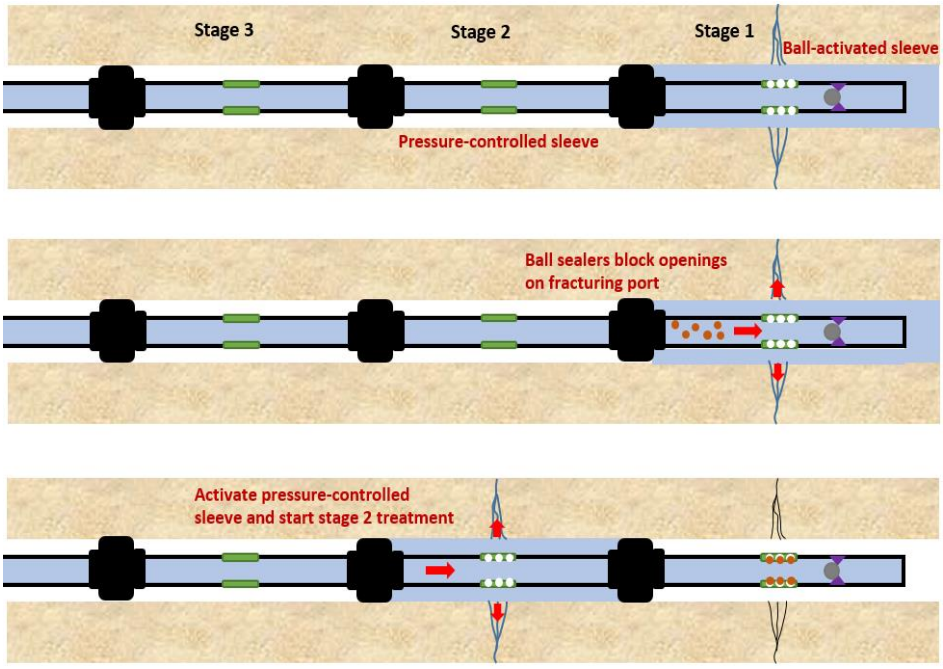

Figure 2.3 – Pressure-controlled sliding sleeve with open-hole packer completion

However, as mentioned in the previous section, ball seating efficiency in a horizontal well is generally very low. This low blockage rate may fail to increase the back pressure to achieve the designed sleeve opening pressure. Eventually, the treating fluids may fail to be placed at the designed interval.

The successful activation of a pressure-controlled sleeve can be diagnosed in several methods. 1) Observe the surface treating pressure response at the time ball sealers arrive at the perforations. 2) Use bottomhole pressure recorded or calculated to determine whether bottomhole pressure reach the required sleeve opening pressure for a specific stage. 3) Use the perforation pressure loss to determine the number of perforations remained open at the end of a stage. If the sliding sleeve is activated and a fracture is created at the corresponding interval, the number of open perforations calculated from perforation pressure loss should matches with the number of perforations on the activated sleeve.

However, the latter two methods require the data for bottomhole pressure, which is defined by,

$$p_{wf} = p_{inj} + \Delta p_{PE} - \Delta p_{f,pipe} \tag{2.20}$$

where p_{inj} is surface treating pressure, Δp_{PE} is hydrostatic pressure drop, and $\Delta p_{f,pipe}$ is tubing friction. When downhole pressure gauge is not installed, the bottomhole pressure needs to be calculated from surface treating pressure. This calculation is largely dependent on the accuracy of job-friction estimation.

2.1.4 Frictional pressure drop prediction

The prediction of frictional pressure drop during a pumping operation is important in calculating bottomhole pressure. In this study, it is assumed that the pressure loss due to tortuosity effect is negligible for an open-hole completion. Therefore, only perforation pressure loss and tubing friction are considered.

The perforation pressure loss can be calculated by (White, 1986),

$$\Delta p_{f,perf} = \frac{1.98244 q^2 \gamma}{N_{perf}^2 K_d^2 d_{perf}^4} \tag{2.21}$$

where q is the injection rate in bpm, γ is the fluid specific gravity, N_{perf} is the number of open perforations, d_{perf} is the diameter of the perforations in inches, and K_d is the discharge coefficient. For fluid without proppant, the discharge coefficient ranges from 0.6 to 1.0, depending on the size and shape of perforation. When a perforation is eroded by proppant flowing through it, the discharge coefficient usually increases. In this study, since no proppant is added in the fluids, a constant discharge coefficient of 0.7 is assumed.

The tubing friction can be calculated from the Fanning equation,

$$\Delta p_{f,pipe} = \frac{2 f_f \rho \left(\frac{q}{A}\right)^2 L}{g_c D} \tag{2.22}$$

where f_f is the Fanning friction factor and can be explicitly solved using (Chen, 1979), when $N_{RE} < 2000$

$$\frac{1}{f_f} = \frac{16}{N_{RE}} \tag{2.23}$$

and when $N_{RE} > 2000$

$$\frac{1}{\sqrt{f_f}} = -4\log\left\{\frac{\varepsilon}{3.7065} - \frac{5.0452}{N_{RE}}\log\left[\frac{\varepsilon^{1.1098}}{2.8257} + \left(\frac{7.149}{N_{RE}}\right)^{0.8981}\right]\right\} \tag{2.24}$$

For Power-Law fluid, generalized Reynolds number should be used,

$$N_{RE}^{'} = \frac{0.249\rho u^{2-n'} D^{n'}}{96^{n'} K'\left[(3n'+1)/4n'\right]^{n'}} \tag{2.25}$$

where *n'* is fluid flow behavior index, and *K'* is consistency index.

When fluid properties are not measured, tubing friction gradient can be estimated from field data. An example is shown to illustrate how to calculate pipe friction gradient at a certain pump rate. **Table 2.1** summarizes the condition for the example, and **Fig. 2.4** shows the field treatment records.

Table 2.1 Parameters used for friction gradient example calculation

Tubing length, ft	15000
Perforation number	40
Perforation diameter, in.	0.394
Discharge coefficient	0.7
Tubing diameter, in.	2.992
Fluid specific density	1

As shown in **Fig. 2.4**, at 60 minutes, the well was shut-in, causing a surface pressure drop of 6000 psi, as the pump rate changed from 31 bpm to 0. The perforation pressure loss is 101 psi as calculated by Eq. 2.21. Assuming other near-wellbore pressure drops are negligible, the tubing friction is 5899 psi. Given the tubing length of 15000 ft, the fluid tubing friction gradient at pump rate of 31 bpm in a 2.992 in. pipe is 0.393 psi/ft.

$$\Delta p_{f,perf} = \frac{1.98244 q^2 \gamma}{N_{perf}^2 K_d^2 d_{perf}^4} = \frac{1.98244 \times 31^2 \times 1}{40^2 \times 0.7^2 \times 0.394^4} \cong 101 psi \tag{2.26}$$

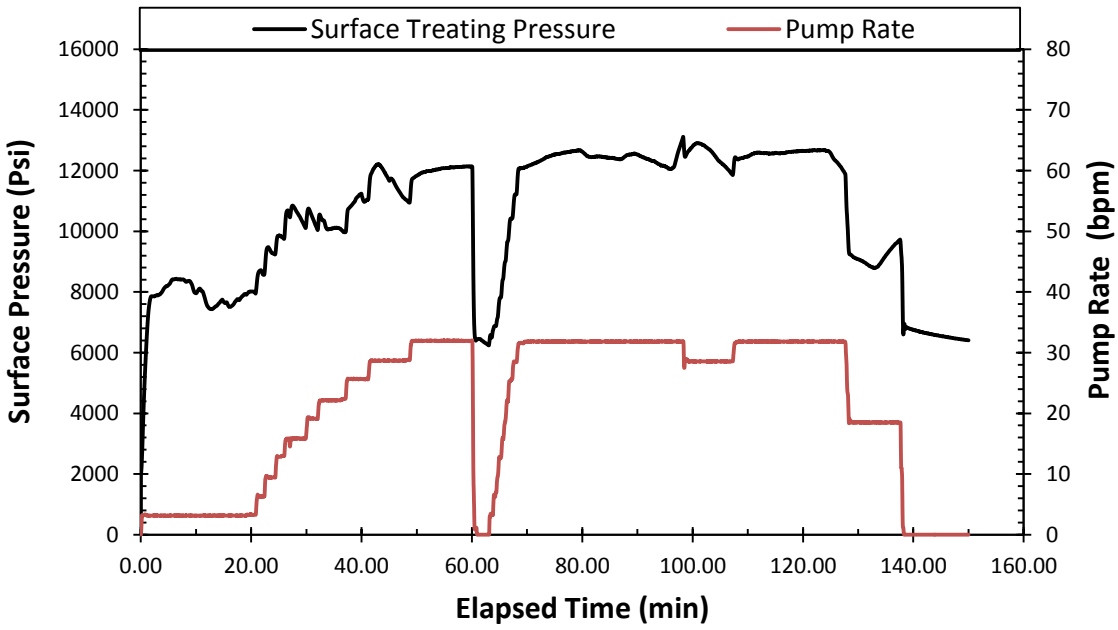

Figure 2.4 – Surface pressure and pump rate records from a field treatment for the example calculation

If enough data are collected, a correlation between injection rate and friction gradient can be generated by curve fitting the data points for certain fluid type in certain pipe diameter. With this correlation, tubing friction for any length of pipe at any pump rate can be calculated.

2.2 Pseudo-3D Fracture Propagation Modeling

An accurate friction prediction is not only helpful in completion design, but also important in predicting fracture dimensions. The fracture propagation process is strongly affected by the net pressure which is related to bottomhole treating pressure. Bottomhole treating pressure, which is the pressure at the reservoir-face is defined by,

$$p_{res-face} = p_{inj} + \Delta p_{PE} - \Delta p_{f,pipe} - \Delta p_{f,perf} \tag{2.27}$$

where $\Delta p_{f,perf}$ is perforation pressure.

The net pressure is the pressure difference between fluid pressure inside a fracture and the pressure acting perpendicular to the fracture wall (formation closure pressure). At fracture entrance, net pressure is expressed as,

$$p_{net} = p_{res-face} - \sigma_c \tag{2.28}$$

Formation closure stress σ_c is usually assumed to be the same as minimum horizontal stress, which can be calculated by (Biot and Willis, 1957),

$$\sigma_{h,\min} = \frac{\upsilon}{1-\upsilon}\left(\sigma_v - \alpha p_p\right) + \alpha p_p \tag{2.29}$$

where υ is the Poisson's ratio, α is the Biot's coefficient, and σ_v is the vertical stress.

Meyer (1986, 1989, and 1990) developed a modified pseudo-3D fracture model, which is used in this study, to simulate fracture geometry of fractures. There are some major assumptions in the modified pseudo-3D model. As illustrated in **Fig. 2.5**, instead of one-dimensional flow, there are two flow directions in this model, which are in fracture length and height directions. The vertical plane strain condition is assumed. The governing equations involved in this pseudo-3D fracture propagation model are presented as the following.

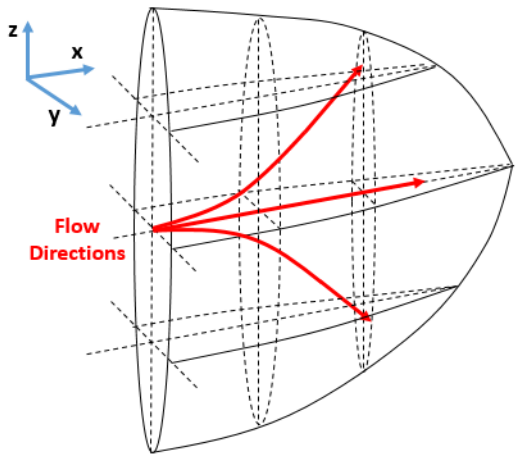

Figure 2.5 – Illustration of Meyer's pseudo-3D fracture model

The governing equations include mass conservation, mass continuity, momentum conservation, fracture width as a function of net pressure, and fracture propagation criteria.

The mass conservation equation for incompressible treating fluids in a fracture is related to the volume change of the treating fluids in the fracture. It is expressed as,

$$\int_0^t q(\tau)d\tau - V_f(t) - V_l(t) - V_{sp}(t) = 0 \tag{2.30}$$

where the first term is the total injected fluid volume till time *t*, $V_f(t)$ is the volume of fluid in the fracture, $V_l(t)$ is the total leak-off volume defined by (Carter, 1957),

$$V_l(t) = 2\int_0^t \int_0^A \frac{C(A,t)}{\left[t-\tau(A)\right]^{\frac{1}{\alpha_\tau}}} dA dt \tag{2.31}$$

$$\tau(A) = t\left[\frac{A}{A(t)}\right]^{\frac{1}{\alpha_a}} \tag{2.32}$$

where fracture surface area $A(t)$ is a function of time, and A is the fracture surface area at time *t*. $\tau(A)$ is the fluid loss delay time which represents the elapsed time from the beginning of the treatment to the time when fracture surface area is $A(t)$. α_τ is the fluid loss power coefficient, and α_a is the leak-off area propagation parameter.

$V_{sp}(t)$ is spurt loss volume defined by,

$$V_{sp}(t) = 2S_p A(t) \tag{2.33}$$

where S_p is the spurt loss coefficient.

The momentum conservation equation can be written as,

$$\rho\frac{D\vec{v}}{Dt} = -\vec{\nabla}p + \left[\vec{\nabla}\cdot\vec{\tau}\right] + \rho\vec{g} \tag{2.34}$$

where on the left-hand side of the equation is the rate change of momentum, and on the right-hand side of the equation are the pressure, viscous and gravitational forces respectively.

The fracture width and net pressure relationship is (Tada et al., 1973),

$$w(x,y)=\int_{-h/2}^{h/2}\Delta p(x,z_0+z')\left(\frac{1-\nu}{\pi G}\right)\ln\left[R_z(z,z')\right]dz' \tag{2.35}$$

where

$$R_z(z,z')=\frac{\left[\left(\frac{h}{2}+z'\right)\left(\frac{h}{2}+z_0-z\right)\right]^{\frac{1}{2}}+\left[\left(\frac{h}{2}-z'\right)\left(\frac{h}{2}-z_0+z\right)\right]^{\frac{1}{2}}}{\left|\left[\left(\frac{h}{2}+z'\right)\left(\frac{h}{2}+z_0-z\right)\right]^{\frac{1}{2}}-\left[\left(\frac{h}{2}+z'\right)\left(\frac{h}{2}-z_0+z\right)\right]^{\frac{1}{2}}\right|} \tag{2.36}$$

where the elevation z is measured from the center of the pay zone, z' is measured from the center of the fracture, and z_0 is the location of the center of the fracture relative to the center of the pay zone, the pressure difference is the net pressure,

$$\Delta p(x,z)=p(x,z)-\sigma(z) \tag{2.37}$$

where $p(x,z)$ is the pressure inside fracture at location (x,z), and $\sigma(z)$ is the formation closure stress of layer at z.

The fracture propagation criteria is based on the concept of a stress intensity factor K_I defined by.

$$K_I=K_{I,\Delta p}+K_{I,\Delta\rho h}+K_{I,\Delta\sigma}+K_{I,G} \tag{2.38}$$

In Eq. 2.38, $K_{I,\Delta p}$ is intensity factor induced by net pressure, $K_{I,\Delta\rho h}$ is intensity factor induced by gravity contrast, $K_{I,\Delta\sigma}$ is intensity factor induced by in-situ stress difference, and $K_{I,G}$ is intensity factor induced modulus contrast. When the stress intensity factor equals or larger than fracture toughness, or the critical stress intensity of the rock K_{Ic}, then the fracture will propagate.

By solving the above governing equations numerically, the fracture propagation solution is obtained.

2.3 Acid Fracture Conductivity Prediction

Acid fracture conductivity is simulated by a 3D acid fracturing model (Oeth et al., 2013). The simulator calculates final acid fracture conductivity profile of an acid-etched fracture under closure stress. It considers both acid transport and reaction. The acid transport model includes the non-Newtonian characteristics of most acid fracturing fluids, the solution for three-dimensional fluid velocity and pressure fields, diffusion of acid toward the fracture surface, and reaction at the fracture surfaces. Furthermore, in this model, the impact of formation heterogeneity is included in the acid fracture conductivity correlation. The model ultimately provides two-dimensional acid fracture conductivity and acid-etched width profiles that can be used in reservoir simulation.

Currently, this acid fracturing simulator does not contain a fracture propagation model. Therefore, to run this simulator, an initial fracture geometry created by a fracture propagation model is needed. In this research, the fracture propagation model used is the pseudo-3D model describe in section 2.3. For multi-stage treatment schedules alternating between pad fluids and acids, all pad fluids pumped are first combined as one injection stage to estimate the initial fracture geometry of the treatment. Then, acid injections are continued to be modeled. The governing equations in this acid fracturing simulator are presented as the following. Assume the same fracture domain and coordinate system in **Fig. 2.5** are applied for this section.

To obtain final fracture conductivity profile, acid-etched width due to acid and rock reaction needs to be calculated first. Acid concentration in the fracture determines how much rock is dissolved for each grid block at fracture surfaces. Tracking acid transport in a fracture is done by first solving fluid velocity field using Navier-Stokes equations (Eq. 2.40 and Eq. 2.43), and then use the fluid velocity field to calculate acid concentration in the fracture using convection-diffusion equation (Eq. 2.51).

The continuity equation,

$$\frac{\partial \rho}{\partial t} + \vec{\nabla} \cdot (\rho \vec{v}) = 0 \tag{2.39}$$

where ρ is the fluid density, $\vec{v}$ is the fluid velocities in three dimensions. Due to the assumption of incompressible fluid, the first term in Eq. 2.45 is dropped, then the equation is simplified as,

$$\vec{\nabla} \cdot \vec{v} = 0 \tag{2.40}$$

The momentum equation,

$$\rho \frac{\partial \vec{v}}{\partial t} + \rho \vec{v} \vec{\nabla} \cdot \vec{v} = -\vec{\nabla} p + \vec{\nabla} \cdot \vec{\vec{\tau}} + \rho \vec{g} \tag{2.41}$$

where $\vec{\vec{\tau}}$ is the viscous stress tensor. For incompressible Newtonian fluid, the divergence of the viscous stress tensor is defined by,

$$\vec{\nabla} \cdot \vec{\vec{\tau}} = \mu \left[\vec{\nabla} \cdot \left(\vec{\nabla} \vec{v} + \left(\vec{\nabla} \vec{v} \right)^T \right) \right] = \mu \vec{\nabla}^2 \vec{v} \tag{2.42}$$

by further assuming steady-state condition, and gravity is neglected, the first and the last terms in Eq. 2.41 are dropped. Rearrange Eq. 2.41, the momentum equation becomes,

$$\rho \vec{v} \vec{\nabla} \cdot \vec{v} = -\vec{\nabla} p + \mu \vec{\nabla}^2 \vec{v} \tag{2.43}$$

For non-Newtonian fluid, since the viscosity is no longer a constant but depends on fluid velocity, the apparent viscosity μ_{app} need to be used. The apparent viscosity is defined by (Bird et al. 1987),

$$\mu_{app} = 2K\left(II_d\right)^{(n-1)/2} \tag{2.44}$$

where II_d is the second invariant of the rate of deformation tensor, then the momentum equation for non-Newtonian fluid is defined by (Oeth, 2013),

$$-\vec{\nabla}p + \mu_{app}\vec{\nabla}^2\vec{v} + 2\vec{\vec{d}}_{ij}\vec{\nabla}\mu_{app} = \rho\left(\vec{v}\cdot\vec{\nabla}\right)\vec{v} \tag{2.45}$$

where d_{ij} is the rate of strain tensor. For more details about the Navier-Stokes equations with power law apparent viscosity model, the reader may refer to the Oeth (2013) dissertation.

The three-dimensional velocity field and pressure profile can be obtained by solving Eq. 2.40 and Eq. 2.43 numerically with boundary conditions as the followings,

at the fracture entrance, the fluid flow rate is,

$$q\big|_{x=0} = q_{inj} = \int v_x\big|_{x=0} dA \tag{2.46}$$

at the fracture tip, the pressure is,

$$p\big|_{x=L} = p_{out} \tag{2.47}$$

at the fracture surfaces ($y= y_1, y_2$) , no-slip condition is applied, and the fluid velocity along fracture width direction equals to fluid leakoff velocity v_L ,

$$v_x\big|_{y=y_1,y_2} = v_z\big|_{y=y_1,y_2} = 0 \tag{2.48}$$

$$v_y\big|_{y=y_1,y_2} = v_L \tag{2.49}$$

at the bottom and top of the fracture ($z=0,H$), the fluid velocities for all dimensions are zero

$$v_x\big|_{z=0,H} = v_y\big|_{z=0,H} = v_z\big|_{z=0,H} = 0 \tag{2.50}$$

The velocity field calculated from Navier-Stokes equations for each time step provides the input velocity for the fluid convection in all three dimensions. The convection-diffusion equation (Eq. 2.51) is used to solve the acid concentration profile assuming that acid diffusion in the fracture length and height directions (x, z) can be neglected compared to the acid diffusion in the width direction (y),

$$\frac{\partial C_D}{\partial t} + v_x \frac{\partial C_D}{\partial x} + v_y \frac{\partial C_D}{\partial y} + v_z \frac{\partial C_D}{\partial z} = \frac{\partial}{\partial y}\left(D_{eff} \frac{\partial C_D}{\partial y} \right) \tag{2.51}$$

where C_D is the dimensionless acid concentration C_A/C_i, C_A is the acid concentration, C_i is the injected acid concentration, D_{eff} is the effective diffusion coefficient.

Acid concentration profile can be solved numerically by defining initial condition and boundary conditions as the followings,

initial condition,

the initial acid concentration is zero everywhere in the fracture,

$$C_D\big|_{t=0} = 0 \tag{2.52}$$

boundary conditions,

at the fracture entrance, the acid concentration is the injected acid concentration,

$$C_D\big|_{x=0} = 1 \tag{2.53}$$

at the bottom and top of the fracture, the acid concentration gradient is zero,

$$\left.\frac{\partial C_D}{\partial z}\right|_{z=0,H} = 0 \tag{2.54}$$

at the fracture surfaces, the acid concentration is determined by acid reaction (Settari, 1993),

$$D_{eff}\frac{\partial C_A}{\partial y} = E_f\left(C_A - C_{eqm}\right)^{n'}\left(1-\phi\right)\Big|_{y_1,y_2} \tag{2.55}$$

where E_f is acid reaction rate constant, C_{eqm} is the equilibrium acid concentration, *n'* is the reaction order constant, and ϕ is porosity.

The acid concentration profile calculated from convection-diffusion equation provides the amount of acid that react with rock at fracture surfaces. The acid-etched width, which is defined by the change of dimension in fracture width direction due to rock dissolution, can be determined by,

$$\frac{\partial y}{\partial t} = \frac{\beta MW_{acid}}{\rho(1-\phi)}\left(f v_L C_A - D_{eff}\frac{\partial C_A}{\partial y}\right) \tag{2.56}$$

where β is the dissolving power of the acid varies with different acid system, MW_{acid} is the molecular weight of the acid, f is the fraction of acid to react before leaking off into the formation, and v_L is the leak-off rate. For the derivation of Eq. 2.56, the reader may refer to the Mou (2009) dissertation.

Once acid etched width is determined, the acid fracture conductivity can be calculated using Mou-Deng conductivity correlation (Deng et al., 2011). The advantage of this correlation is that it accounts for the heterogeneity of the formation through three geostatistical parameters. The correlation is defined by,

$$wk_f = C_1 \exp\left(-C_2 \sigma_c\right) \tag{1.1}$$

where C_1 is defined by,

$$\begin{aligned} C_1 = {} & 4.48\times10^9 \left[0.1756\left(erf\left(0.8\sigma_D\right)\right)^3 w_i^{2.49}\right] \\ & \times\left[1+\left(1.82erf\left(3.25\left(\lambda_{D,x}-0.12\right)\right)-1.3erf\left(6.71\left(\lambda_{D,z}-0.03\right)\right)\right)\right. \\ & \left.\times\sqrt{\exp\left(\sigma_D\right)-1}\right]\times\left[0.22\left(\sigma_D\lambda_{D,x}\right)^{2.8}+0.01\left(\sigma_D-\sigma_D\lambda_{D,z}\right)^{0.4}\right]^{0.52} \end{aligned} \tag{2.57}$$

and C_2 is defined by,

$$C_2 = \left[14.9-3.78\ln\left(\sigma_D\right)-6.8\ln\left(E\right)\right]\times10^{-4} \tag{2.58}$$

where σ_c is the formation closure stress, $\lambda_{D,,x}$, $\lambda_{D,,z}$, and σ_D are the three geostatistical parameters representing dimensionless horizontal correlation length, dimensionless vertical correlation length, and dimensionless standard deviation of permeability respectively, and w_i is the acid-etched width at zero closure stress.

The two dimensionless correlation lengths describe how continuous permeability is distributed in horizontal and vertical directions. A more homogeneous formation will show larger dimensionless correlation lengths in both directions. If the permeability is discontinuous, then smaller dimensionless correlation length value will be obtained. Dimensionless correlation length is calculated by using variogram of permeability distribution along fracture height and length directions and it is defined by,

$$\gamma\left(h\right) = \frac{1}{2N}\sum\left(z_i - z_{i+h}\right)^2 \tag{2.59}$$

where N is the number of data pairs in the data set, z_i is one data point and z_{i+h} is another data point that is h distance away from z_i. The correlation length is the distance where the

variance γ(h) is reaching plateau. The dimensionless correlation length is then the ratio of correlation length to the entire data range interval.

The dimensionless standard deviation of permeability σ_D is defined by,

$$\sigma_D = \frac{\sigma(\ln(k))}{\ln(\bar{k})} \tag{2.60}$$

where *σ(ln(k))* is the standard deviation of the natural logarithm of permeability *k*, and $\bar{k}$ is the average permeability.

2.4 Post-treatment Production Prediction

The advantage of having a 2D fracture conductivity profile is that fracture properties can be assigned to fracture grids that are coupled with reservoir grids for reservoir simulation. However, when use analytical productivity model for production prediction, only an average fracture conductivity is required. The average fracture conductivity can be calculated as the arithmetic average over the fracture area.

If the dimensionless fracture conductivity is larger than 50, and the reservoir is assumed as a rectangular shape, as shown in **Fig. 2.6**, then the linear flow model developed by Wattenbarger et al. (1998) can be applied to calculate production rate for both early transient period and late depletion period.

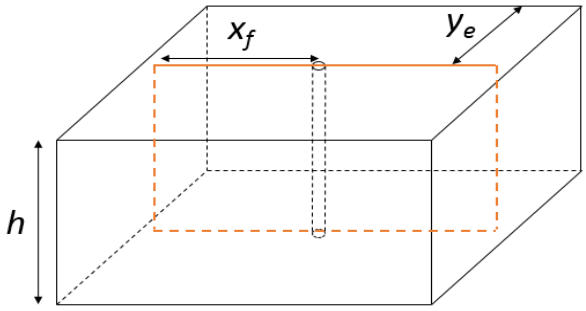

Figure 2.6 – A vertically fractured well in a rectangular reservoir

The solution for gas flow requires the differential real gas pseudo-pressure defined by,

$$\Delta m(p) = 2\int_{p_{wf}}^{p_i} \frac{p}{z\mu} dp \approx \frac{p_i^2 - p_{wf}^2}{\mu Z} \tag{2.61}$$

For a constant bottomhole flowing pressure production from a closed linear reservoir, the solution is,

$$\frac{1}{q_D} = \frac{\frac{\pi}{4}\left(\frac{y_e}{x_f}\right)}{\sum_{n=1}^{\infty} \exp\left(-\frac{(2n-1)^2\pi^2}{4}\left(\frac{x_f}{y_e}\right)^2 t_{Dx_f}\right)} \tag{2.62}$$

where the dimensionless production rate is defined by,

$$\frac{1}{q_D} = \frac{kh\left[m(p_i) - m(p_{wf})\right]}{1424 q_g T} \tag{2.63}$$

and

$$t_{Dx_f} = \frac{0.0002637kt}{\phi\mu c_t x_f^2} \tag{2.64}$$

Another dimensionless variable t_{Dy_e} is introduce in order to determine when the end of early transient period is. For the constant bottomhole flowing pressure case, if t_{Dy_e} is larger than 0.25, then the transition from transient flow to pseudosteady state flow starts. t_{Dy_e} is defined by,

$$t_{Dy_e} = \frac{0.0002637kt}{\phi\mu c_t y_e^2} = \left(\frac{x_f}{y_e}\right)^2 t_{Dx_f} \tag{2.65}$$

For a short-term (transient period, $t_{Dy_e} < 0.25$) prediction, the solution of dimensionless gas rate shown in Eq. 2.62 can be approximate by,

$$\frac{1}{q_D} = \frac{\pi}{2}\sqrt{\pi t_{Dx_f}} \tag{2.66}$$

For a long-term (depletion period, $t_{Dy_e} > 0.25$) prediction, the solution of dimensionless gas rate shown in Eq. 2.62 can be approximate by,

$$\frac{1}{q_D} = \frac{\pi}{4}\left(\frac{y_e}{x_f}\right)\exp\left(\frac{\pi^2}{4}t_{Dy_e}\right) \tag{2.67}$$

Wattenbarger et al. (1998) also showed the equation for productivity index for long-term production forecast under constant bottomhole flowing pressure,

$$J = \frac{q_g}{m(p) - m(p_{wf})} = \frac{kh}{1424T\left[\frac{2}{\pi}\left(\frac{y_e}{x_f}\right)\right]} \tag{2.68}$$

For a horizontal well with *n* transverse fractures as illustrated in **Fig. 2.7**, the total productivity of a fractured well is,

$$J_{total} = \sum_{i=1}^{n} J_i \tag{2.69}$$

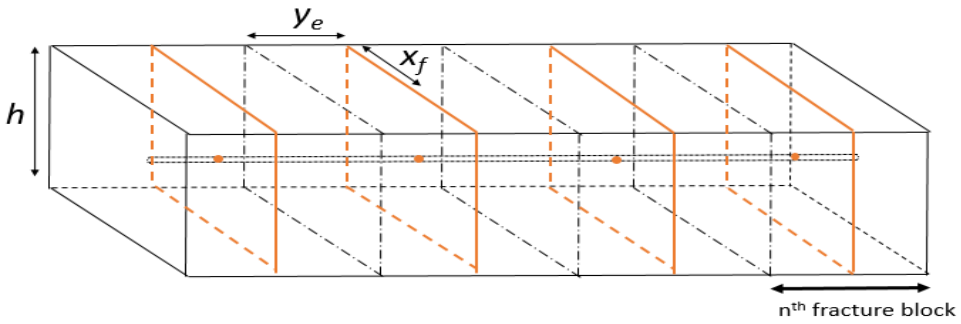

Figure 2.7 – A horizontal well with multiple transverse fractures

The productivity index of untreated horizontal wells under pseudosteady-state condition is calculated using the Babu & Odeh model (1988, 1989).

$$J_H = \frac{q_g}{m(p) - m(p_{wf})} = \frac{\sqrt{k_x k_z}\, b}{1424T\left[\ln\left(\frac{A^{0.5}}{r_w}\right) + \ln C_H - 0.75 + s_R + s\right]} \tag{2.70}$$

where k_x and k_z are the horizontal and vertical permeability, b is the reservoir length in the well direction, A is the reservoir cross-sectional area perpendicular to the well direction, r_w is the wellbore radius, C_H is the shape factor and s_R is the partial penetration skin. The definitions of these two functions can be found in Babu & Odeh's original work

(1988, 1989). The productivity index ratio of fractured well to un-fractured well can be calculated by Eq. 2.68 - Eq. 2.70,

$$\frac{J_{total}}{J_H} = \frac{1424T\left[\ln\left(\frac{A^{0.5}}{r_w}\right) + \ln C_H - 0.75 + s_R + s\right]\sum_{i=1}^{n} J_i}{\sqrt{k_x k_z}\, b} \tag{2.71}$$

2.5 Model Integration

To develop a comprehensive approach to predict performance of multi-stage acid fracturing treatment in horizontal wells, evaluation of each component from the previous sections needs to be integrated. The approach of evaluating such a complex process is demonstrated in **Fig. 2.8**. The blue boxes represent processes for completion evaluation, the orange boxes represent processes for acid fracturing simulation, and the green boxes represent process for production prediction.

As shown in **Fig. 2.8**, well completion design, which includes stage isolation methods, friction prediction, and bottomhole pressure calculation, is first evaluated. The evaluation of stage isolation determines the number and locations of fractures that are created in the treatment. Failure of fracture initiation needs to be identified, so that actual fluid placement during the treatment can be determined. The prediction of frictional pressure drop can be done either by known fluid properties or from friction gradient generated from surface pressure records.

With recorded surface pressure, and calculated tubing friction and perforation pressure loss during pumping, bottomhole treating pressure can be calculated. Formation stress can be interpreted from logging data if no calibration tests have been done before the main treatment. Rock mechanical properties are also interpreted from logs. Together

with fluid placement from well completion evaluation and treatment schedule, fracture geometry can be simulated using a fracture propagation model. Pressure history match will be performed to determine whether the simulation results are consistent with the treatment records.

The output fracture geometry is the input for the acid transport and reaction models. The fracture dimensions, which are used to define the model boundary, are discretized into a three-dimensional grid system. Each grid has the same length and height, but may have different width. Once the acid-etched width for grids at the fracture surface are calculated, an acid fracture conductivity correlation can be used to generate the acid fracture conductivity profile.

The simulated fracture dimensions and conductivity are used in a productivity model for vertically fracture wells for post-treatment production prediction.

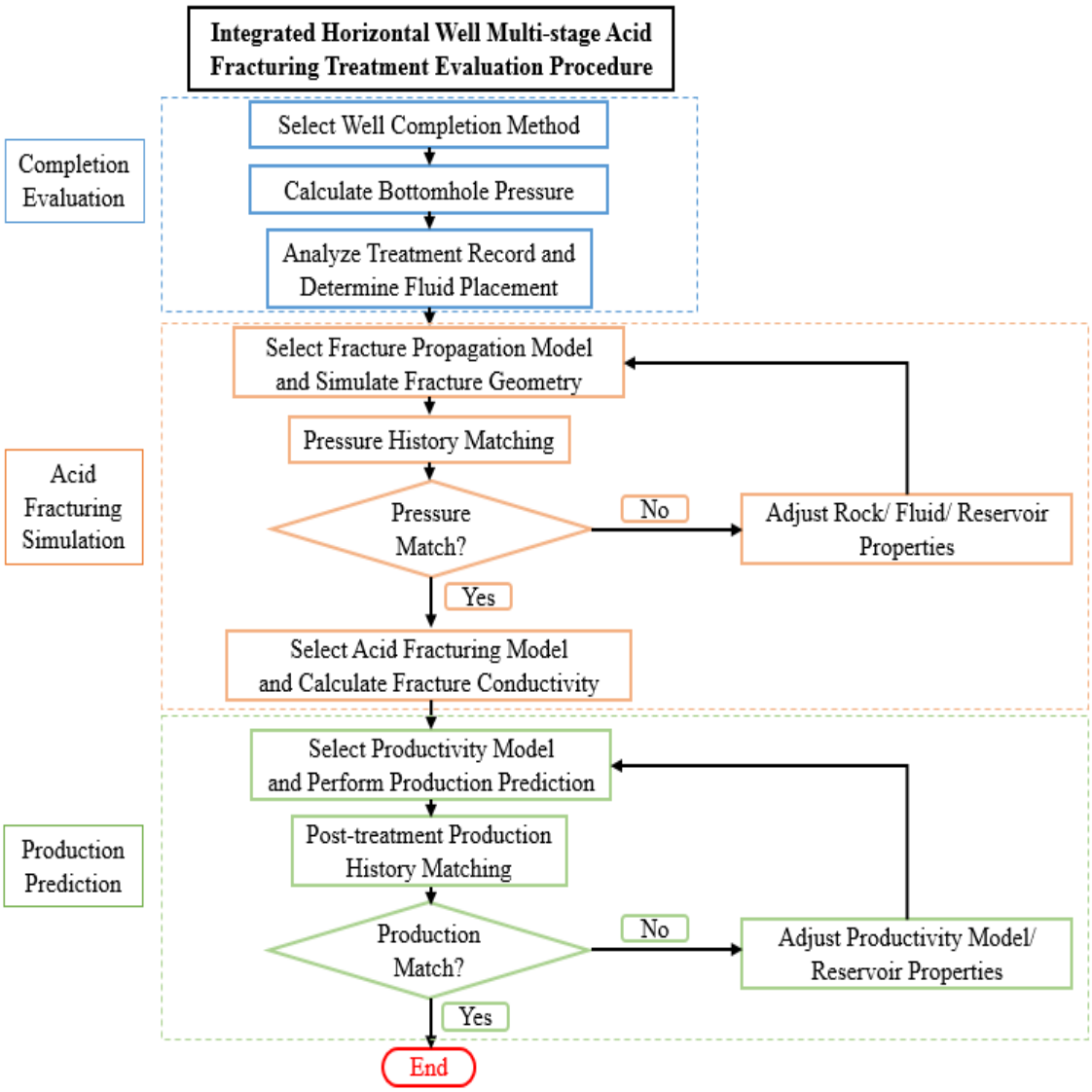

Figure 2.8 – Integrated multi-stage acid fracturing treatment evaluation work flow

CHAPTER III

FIELD APPLICATION

In this chapter, a post-job evaluation of an acid fracturing in a carbonate reservoir is presented. The evaluation using the integrated approach is based on actual field data. Results of the evaluation are discussed.

3.1 Treatment Description

Well A is a horizontal well drilled in a gas condensate carbonate reservoir. The vertical depth of the well is approximately 17818 ft. The formation pressure and temperature are predicted to be 9985 psi and 300 ˚F respectively. The formation breakdown pressure at the target depth is estimated to be 16040 psi from the drilling records. The well is completed for a 6-stage acid fracturing stimulation performed over 2560 ft of the horizontal lateral section. Permeability and porosity tests were conducted on the core plugs. Additionally, well logs including density log, acoustic log, and gamma log were provided for analysis on Young's Modulus and Poisson's ratio. **Table 3.1** summarizes the reservoir and well stimulation data.

Table 3.1 Summary of well stimulation and reservoir data

Well stimulation data	
Completion method	Open-hole
Isolation method	Pressure-controlled sleeve
Vertical depth of the stimulation interval, ft	17818
Total stimulation interval length, ft	2560
Tubing size, in.	2.992
Total number of stages designed	6
Reservoir data	
Formation pressure, psi	9985
Formation temperature, ˚F	300
Breakdown pressure, psi	16040
Matrix permeability, mD	0.0044
Matrix porosity	0.02
Average Young's Modulus, MMpsi	8
Average Poisson's ratio	0.3

Treatment fluids include gelled acid, crosslinked acid, and fracturing fluid. A total volume of 523060 gallons of the fracturing fluid, 129444 gallons of the gelled acid, and 221900 gallons of the crosslinked acid were pumped. The HCL concentrations for both acids are 20%. The apparent viscosity for the fracturing fluid is 60 cp, for gelled acid is 30 cp, and for crosslinked acid is 42 cp. The specific density for the fracturing fluid is 1.0, for gelled acid is 1.1, and for crosslinked acid is 1.1. The fracturing fluid and acids were injected alternatively as shown in **Table 3.2**. During the treatment operation, the surface treating pressure and pump rate were recorded. The maximum surface pressure and pump

rate achieved are 13240 psi and 41 bpm. No bottomhole pressure gauge was installed, therefore bottomhole pressure during the treatment needs to be calculated from the surface treating pressure. Well A was stimulated right after the completion. No pre-treatment production is available. The post-treatment production was recorded for the first 113 days after the multi-stage acid fracturing treatment.

Table 3.2 Treatment schedule for Well A multi-stage acid fracturing stimulation

Stage 1 schedule		
Injection sequence	Fluid Type	Volume gal
1	Gelled Acid	18492
2	Crosslinked Acid	31700
3	Fracturing Fluid	52834
4	Crosslinked Acid	36984
5	Fracturing Fluid	52834
6	Gelled Acid	18492
7	Shut-in	
Stage 2 schedule		
Injection sequence	Fluid Type	Volume gal
1	Fracturing Fluid (drop 50 ball sealers)	13737
2	Gelled Acid	10567
3	Crosslinked Acid	15850
4	Fracturing Fluid	47551
5	Crosslinked Acid	18492
6	Fracturing Fluid	2375
7	Gelled Acid	10567

Table 3.2 Continued

Stage 3 schedule		
Injection sequence	Fluid Type	Volume gal
1	Fracturing Fluid (drop 50 ball sealers)	12231
2	Gelled Acid	10567
3	Crosslinked Acid	13209
4	Fracturing Fluid	39626
5	Crosslinked Acid	21134
6	Fracturing Fluid	31701
7	Gelled Acid	7925
Stage 4 schedule		
Injection sequence	Fluid Type	Volume gal
1	Fracturing Fluid (drop 54 ball sealers)	10567
2	Gelled Acid	7925
3	Crosslinked Acid	15850
4	Fracturing Fluid	34342
5	Crosslinked Acid	13209
6	Fracturing Fluid	21134
7	Gelled Acid	7925
Stage 5 schedule		
Injection sequence	Fluid Type	Volume gal
1	Fracturing Fluid (drop 55 ball sealers)	10567
2	Gelled Acid	10567
3	Crosslinked Acid	18492
4	Fracturing Fluid	34342
5	Crosslinked Acid	18492
6	Fracturing Fluid	31701
7	Gelled Acid	10567

Table 3.2 Continued

Stage 6 schedule		
Injection sequence	Fluid Type	Volume gal
1	Fracturing Fluid (drop 55 ball sealers)	10567
2	Gelled Acid	7925
3	Crosslinked Acid	10567
4	Fracturing Fluid	21134
5	Crosslinked Acid	7925
6	Fracturing Fluid	15850
7	Gelled Acid	7925
8	Flush	6868

The evaluation procedure made by the integrated acid fracturing treatment evaluation model for this particular field treatment is shown in **Fig. 3.1**. The shadowed blocks represent models selected for this particular treatment from the integrated evaluation approach.

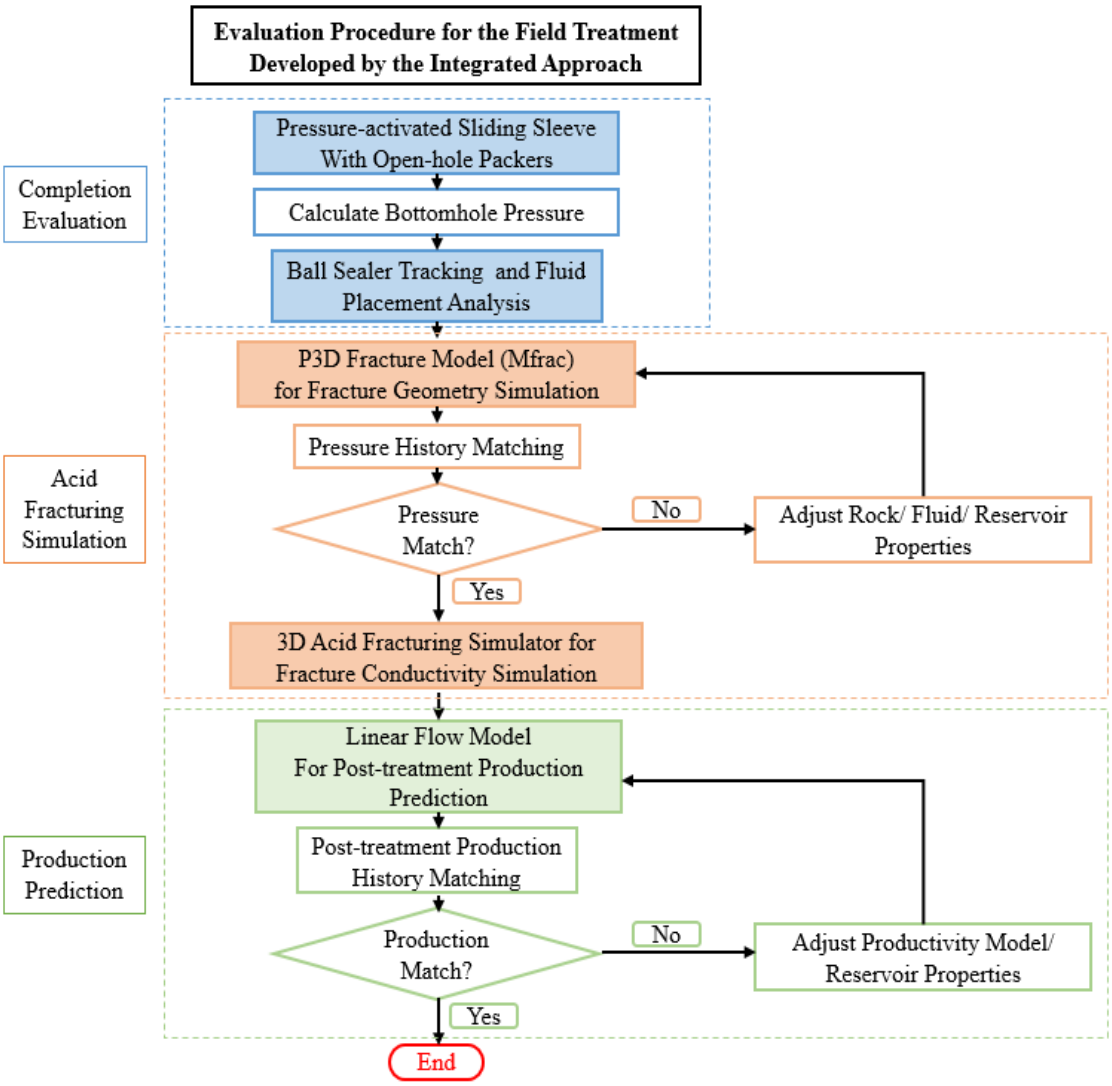

Figure 3.1 – Procedure for field multi-stage acid fracturing treatment evaluation

3.2 Completion Evaluation

The well is completed using a combination of ball-activated and pressure-controlled sliding sleeves with open-hole packers for the multi-stage treatment. Only the first stage is designed with ball-activated sleeve, and the rest of the stages use pressure-

controlled sleeves and ball sealers for stage isolation. Each fracture port has 40 perforations with a 0.394 in. diameter. According to the completion design, the critical bottomhole pressures required to activate sleeves from stage 1 to stage 6 are summarized in **Table 3.3**.

Table 3.3 Critical bottomhole pressure to open each sleeve

Stage	Sleeve	Sleeve Type	Critical BHP to open sleeve (psi)
1	1	Ball-activated	13300
2	2	Pressure-controlled	16133
3	3	Pressure-controlled	16900
4	4	Pressure-controlled	16900
5	5	Pressure-controlled	17670
6	6	Pressure-controlled	17670

In order to determine the fluid placement for each stimulation interval, it is important to know if all sleeves were successfully activated as designed which requires a calculation of bottomhole pressure during the treatment.

3.2.1 Treatment bottomhole pressure calculation

Since the fluid Power-Law properties were not measured, the fluid tubing friction cannot be calculated using Eq. 2.22. However, from surface treating pressure changes due to well shut-ins or abrupt pump rate changes, we can estimate the fluid tubing friction using the method illustrated in section 2.1. As shown in **Fig. 3.2**, each data point

corresponds to a tubing friction gradient estimated from a field measurement for a certain fluid type. With trend lines fitting the data points, one can predict the tubing friction of any fluid for any pipe length at any injection rates. Theoretically, the Power-Law fluid properties, flow behavior index *n'* and consistency index *K'*, can be backed out from a friction gradient curve, using Eq. 2.22 – Eq. 2.25 by assuming a pipe roughness. Unfortunately, in this case study, there is no combination of those two parameters can be found to match the fluid tubing friction estimated from the field measurements. Therefore, except for the tubing friction calculation which is based on the friction correlations generated from the field data, the fluids are treated as Newtonian fluids with apparent viscosities measured from laboratory tests. In all other calculations, apparent viscosity for gelled acid is 30 cp, for crosslinked acid is 42 cp, and for fracturing fluid is 60 cp.

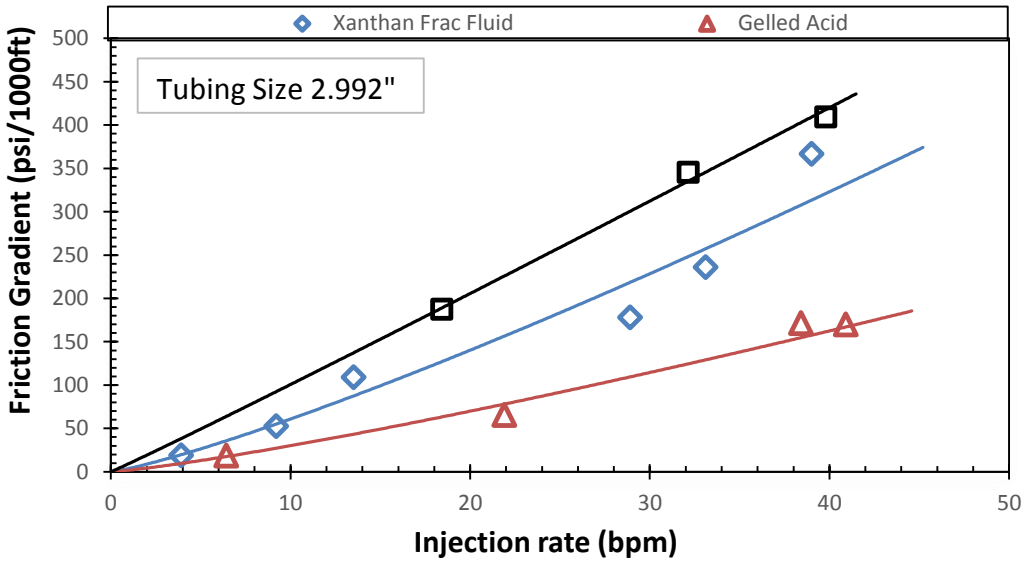

Figure 3.2 – Tubing friction gradient for each treating fluid from field data

Fig. 3.3 shows the bottomhole pressure calculated from the surface treating pressure for all six stages by considering the hydrostatic pressure and tubing friction calculated during the treatment. The treatment record for each stage is separated by the dash lines.

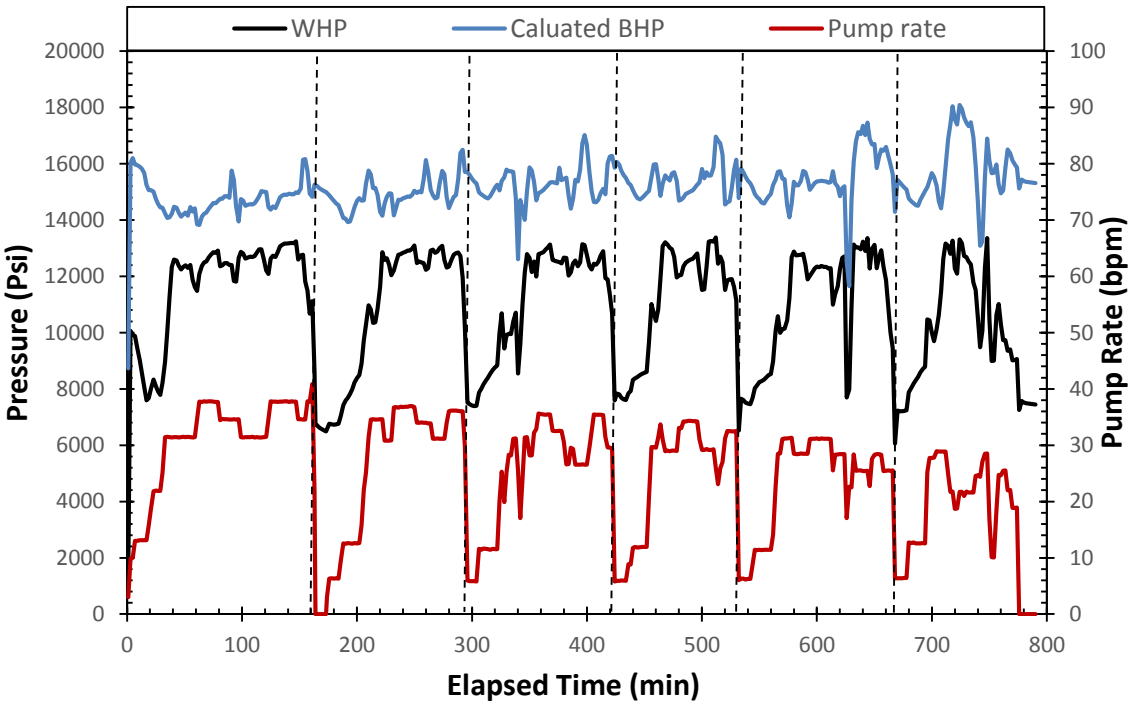

Figure 3.3 – Recorded surface treating pressure, calculated bottomhole pressure and pump rate for all six stages

3.2.2 Ball sealer tracking and sleeve activation

According to the field report, the first sliding sleeve was activated before the main treatment began. After the first stage was finished, 50 ball sealers were dropped with fracturing fluid into the wellbore to block the 40 perforations on sleeve 1. The ball sealer has a specific density of 1.0, which is the same as the carrying fluid. Assume that the ball sealers were injected one at a time, the terminal velocities of the neutral buoyant ball sealer in both vertical and horizontal sections of the well are 0 ft/min by Eq. 2.1. Therefore the actual velocity of the ball sealers is approximately the same as the fluid velocity.

Fig. 3.4 shows stage 2-6 treatment records and the arrival times for ball sealers dropped at each stage in their corresponding stages. However, from the records, no abrupt pressure responses were observed when ball sealers arrived at the perforation intervals. The smooth rise of surface treating pressure during the time period of 190 to 200 minutes, 310 to 317 minutes, 440 to 450 minutes, 550 to 560 minutes, and 685 to 695 minutes were due to increasing tubing friction caused by alternating the gelled acid to the fracturing fluid in the tubing. Furthermore, it is observed that the bottomhole pressures are not high enough to activate the pressure-controlled sleeves of the corresponding stages during the injection.

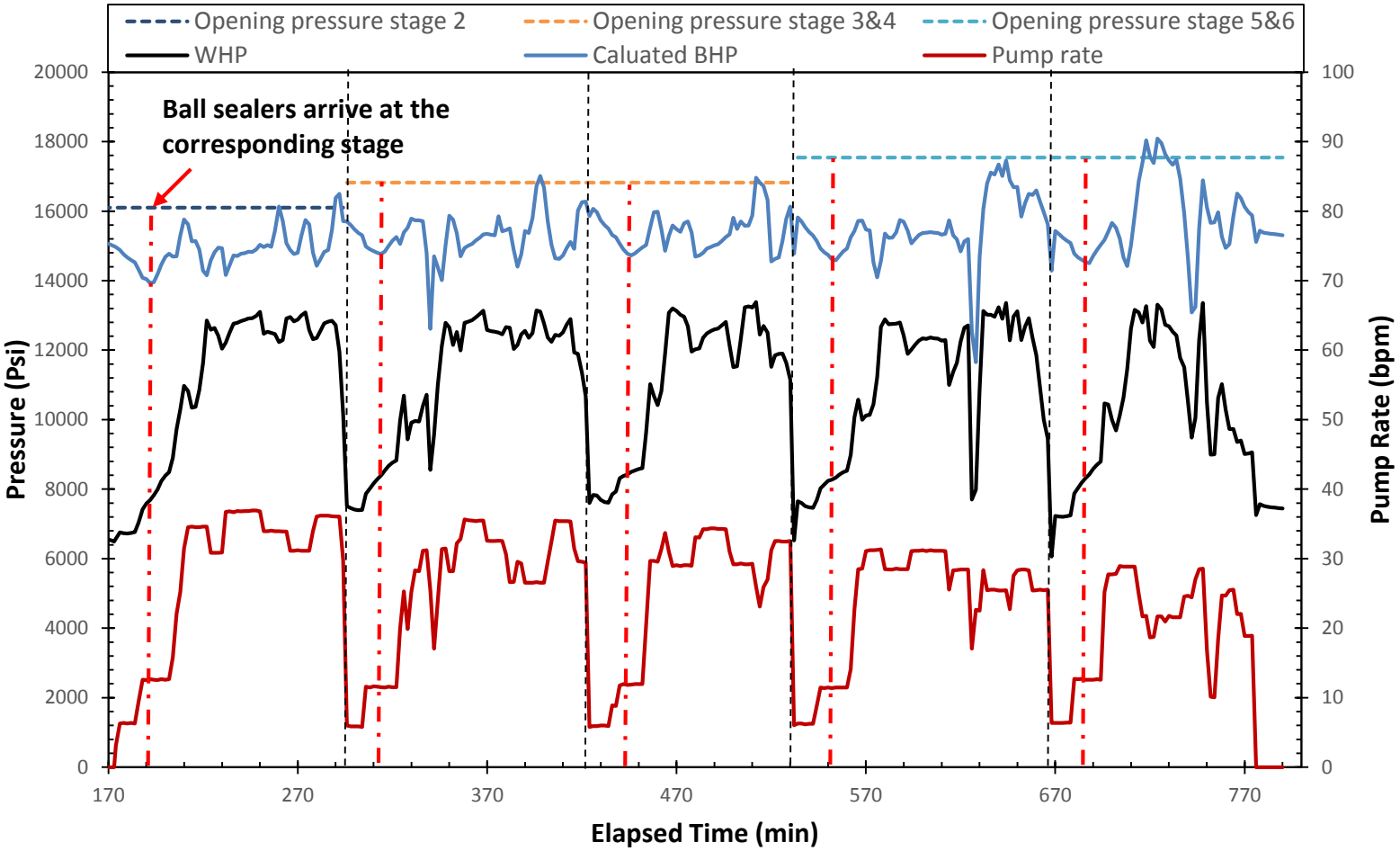

Figure 3.4 – Stage 2-6 treatment records with the calculated bottomhole pressure and the ball sealers arrival times

Another indication of the failure of sleeves opening is an increase in near-wellbore pressure loss as the treatment was carried out. It is observed that even with a decreasing pump rate for each stage stimulation, the perforation pressure loss still increased dramatically. If a sleeve were activated during the treatment and a new fracture was initiated at its corresponding stage, the treating fluids would tend to flow into the newly opened fracture due to less resistance, and this would result in a less pressure. In such condition, the number of open perforations calculated from the shut-in pressure drop should not be less than the number of perforations on the sleeve, which is 40 in this case.

Table 3.4 summarizes the number of open perforations calculated from Eq. 2.21. Pump rate 1 and 2 represent the pump rate right before and after the rate change at the end of each stage. A constant discharge coefficient of 0.7 is used for this calculation. From When N_{perf} is close to 40, it indicates that the sleeve was open as designed. Noticed from **Table 3.4**, after the first stage, N_{perf} is less than 40. This is consistent with the observation of increased pressure. Obviously, the sleeves were not activated as expected. An example of calculating the number of open perforations at the end of stage 1 treatment is shown. Treatment records for stage 1 are shown in **Fig. 3.5**.

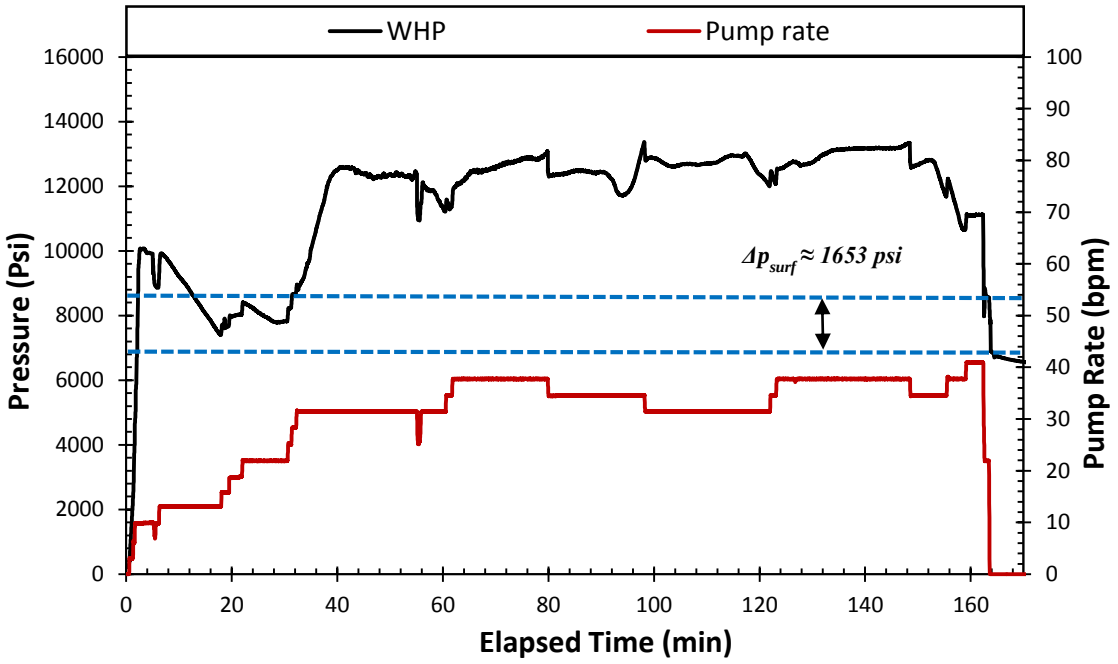

Figure 3.5 – Detailed treatment records for stage 1

From treatment pressure record of stage 1, the surface treating pressure before shut-in was 8555 psi, and after shut-in the surface treating pressure was 6902 psi. Thus the total frictional pressure drop is

$$\Delta p_{f,total} = 8555 - 6902 = 1653 psi \tag{3.1}$$

The corresponding pump rate change is from 22 bpm to 0. At the end of stage 1 injection, the pipe was filled with gelled acid. From **Fig. 3.2**, for gelled acid, the friction gradient at 22 bpm is 78.5 psi/1000ft, knowing the location of stage 1 sleeve is at measured depth of 20360 ft, the tubing friction can be calculated as,

$$\Delta p_{f,pipe} = \frac{78.5 \times 20360}{1000} = 1598 psi \tag{3.2}$$

Assuming no other pressure drops, such as pressure drop due to tortuosity, are considered, the perforation pressure drop then can be calculated as the total frictional pressure drop minus tubing friction,

$$\Delta p_{f,perf} = 1653 - 1598 = 55 psi \tag{3.3}$$

Using Eq. xxx and Eq. xxx, the total number of open perforation at the end of stage 1 can be obtained,

$$\Delta p_{f,perf} = \frac{1.98244 q_1^2 \gamma}{N_{perf}^2 K_d^2 d_{perf}^4} - \frac{1.98244 q_2^2 \gamma}{N_{perf}^2 K_d^2 d_{perf}^4} \tag{3.4}$$

$$N_{perf} = \left(\frac{1.98244 \left(q_1^2 - q_2^2 \right) \gamma}{N_{perf}^2 K_d^2 d_{perf}^4} \right)^{0.5} = \left(\frac{1.98244 \times \left(22^2 - 0 \right) \times 1.1}{55 \times 0.7^2 \times 0.394^4} \right)^{0.5} \cong 40 \tag{3.5}$$

Table 3.4 Number of open perforations at end of each stage treatment

Stage	Pump Rate 1	Pump Rate 2	$\Delta p_{f,total}$	$\Delta p_{f,pipe}$	$\Delta p_{f,perf}$	# of open
	bpm	bpm	psi	psi	psi	perfs
1	22.00	0.00	1653	1598	55	40
2	29.60	5.66	2102	1987	115	37
3	29.88	5.98	2175	1993	182	29
4	32.46	6.29	3194	2217	977	14
5	25.47	6.29	2147	1562	585	14
6	25.41	22.01	580	305	275	10

From completion evaluation based on Well A treatment design and field operation records, it is concluded that only one fracture at the ball-activated sliding sleeve location (stage 1) was created during this treatment.

3.3 Fracture Propagation Simulation and Pressure History Matching

To model the fracture propagation during treatment, the formation and rock mechanical properties need to be calculated. The lithology of the formation is first interpreted from the well logs. The formation closure stress distribution is then calculated using Eq. 2.29 with an average Biot's coefficient of 0.8 and the density value for each lithology is shown in **Table 3.5**. The Young's Modulus and Poisson's ratio were also calculated based on well logs. **Fig. 3.6** shows the calculated formation closure stress and rock properties. From the figure, the local formation closure stress is approximately 14645 psi, average Young's Modulus is approximately 8 MMpsi, and average Poisson's ratio is approximately 0.3 at the target depth (17818 ft).

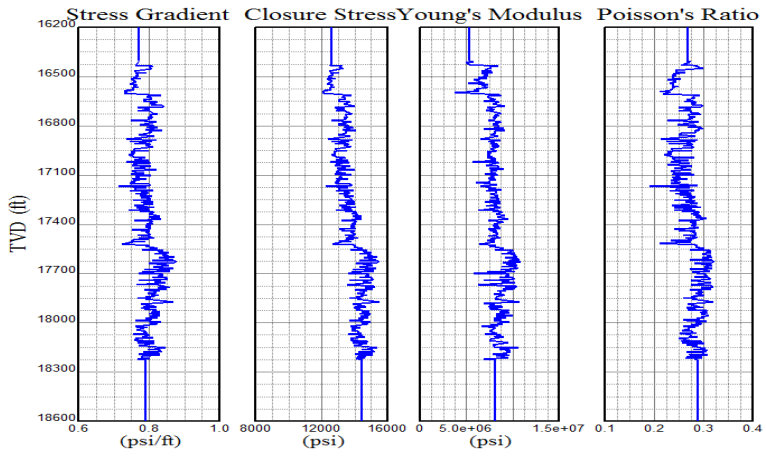

Figure 3.6 – Formation closure stress and rock properties calculated from logs

Table 3.5 Density value for each lithology

Lithology	Density (lbm/ft^3)
Dolomite	181
Limestone	169
Sand	165.4
Shale	156

In **Fig. 3.7,** both calculated bottomhole treating pressure and formation closure stress are presented. When the bottomhole treating pressure falls below the formation closure stress, the fracture starts to close. It is noticed that during this field treating process the fracture was not kept open.

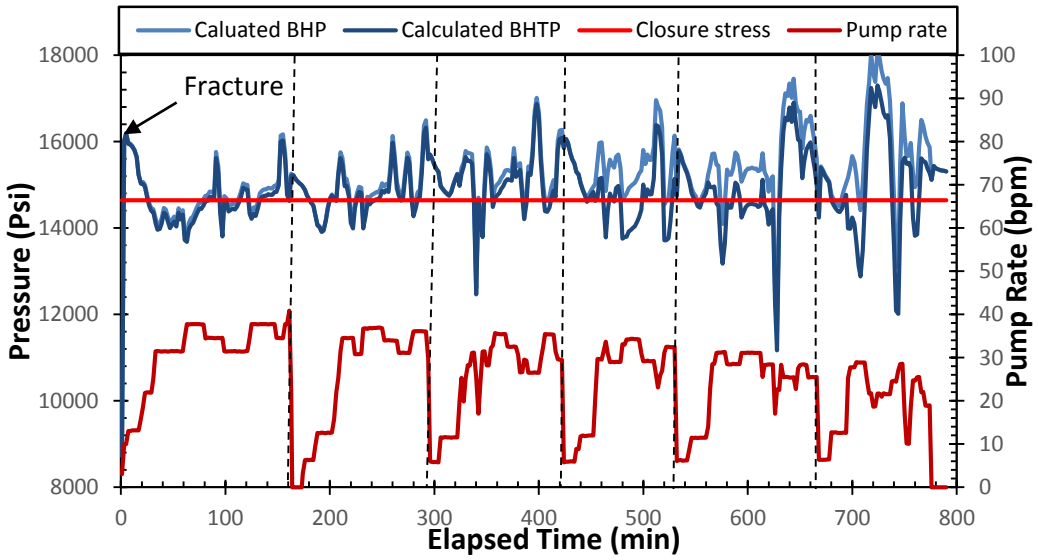

Figure 3.7 – Calculated bottomhole treating pressure and formation closure stress

Because it is believed that only one stage of injection created a fracture, we only simulated on fracture propagation. We also assumed that the fracture only propagated when the bottomhole treating pressure was above the formation closure stress in this field treatment. All fracturing fluid were combined as one continuous injecting stage. A commercial software MFrac (Meyer, 1986, 1989, 1990), which is based on the pseudo-3D model described in section 2.2, was used for generating the final fracture geometry.

The input data in MFrac are composed by 5 sections, including wellbore hydraulics, zones, treatment schedule, rock properties, and fluid loss data. Stress profile, Young's modulus, and Poisson's ratio can be referred to **Fig. 3.6**. Treatment schedule for each stage as shown in **Table 3.2** is input in MFrac with time step of one minute. The leak-off coefficient of the fluids are approximate from the experimental results. Details of input data are shown in **Table 3.6**.

Table 3.6 Summary of MFrac input data

Reservoir data	
Injection method	Through tubing
Sleeve location (MD), ft	20360
Sleeve location (TVD), ft	17818
Number of perforations	40
Diameter of perforations, inch	0.394
Formation permeability, mD	0.0044
Gelled acid leak-off rate, ft/min$^{1/2}$	0.004
Crosslinked acid leak-off rate, ft/min$^{1/2}$	0.004
Fracturing fluid leak-off rate, ft/min$^{1/2}$	0.005

Fig. 3.8 shows that at the end of the treatment the fracture has a half-length of 186 ft, and the maximum width is about 0.11 inches. This fracture geometry is further used as the physical domain for acid transport and reaction simulation.

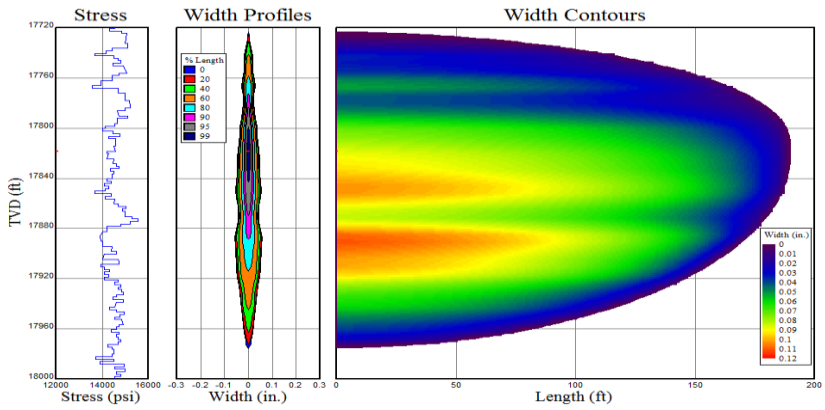

Figure 3.8 – Fracture geometry for acid fracturing simulation

A history match of stimulation pressure responses was conducted for the purpose of verifying the modeling results compared to the field treatment records. It also helps to quantify various effects during the treatment, such as rock mechanical and formation properties, treatment fluid properties. The bottomhole pressure and surface treating pressure from fracture propagation simulation was compared with the bottomhole pressure calculated and surface treating pressure from operational records, and the results are shown in **Fig 3.9**. Overall, the pressure from the fracture simulation matches with the treatment records.

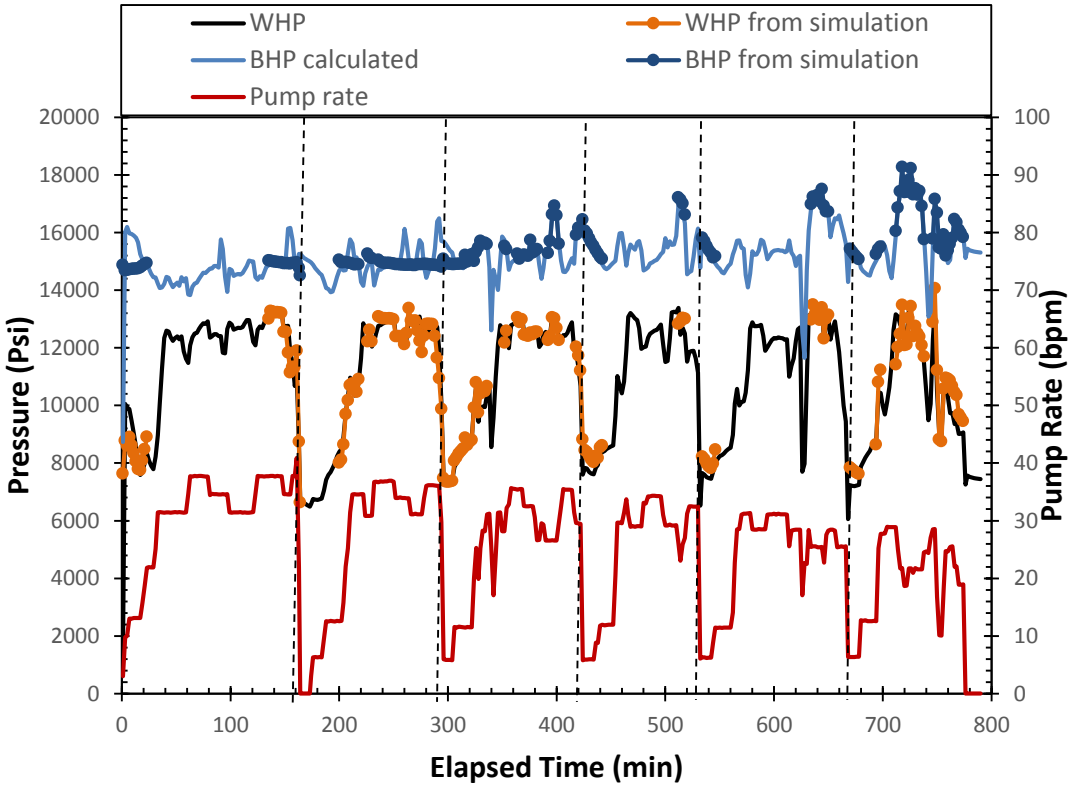

Figure 3.9 – A history match of stimulation pressure responses

3.4 Acid Fracture Conductivity Prediction

The fracture geometry created in section 3.3 were discretized into an 8×6 griding system, and were imported to the acid fracture simulator. Each grid has a length of 23.1 ft, a height of 38.6 ft, so that the total domain matches the initial fracture dimensions from the fracture simulation. All of the acid fluids were combined and simulated as one continuous injection stage following the fracture propagation. Since in this field case the fracture net pressure was not constantly positive, it is assumed that once fracture closes, the acid injected was treating the formation as matrix acidizing instead of acid fracturing. This assumption reduces the total acid volume used in acid fracturing simulation to be 10800 gallons.

Since the the Power-Law properties for the fluids were not measured, and could not be calculated from the friction data, the acid fluids are treated as Newtonian fluids for this case. The dominant mineralogy of the formation is calcite, and the permeability of the formation is 0.0044 mD. Dimensionless vertical correlation length and dimensionless standard deviation of permeability can be calculated from the permeability distribution along the vertical direction interpreted from the well logs. Other input parameters are shown in **Table 3.7**.

Table 3.7 Input parameters for acid fracturing simulator

Newtonian viscosity, cp	30
Fluid density, lb/ft^3	68.6
Formation porosity, fraction	0.02
Acid concentration, wt%	20
Effective diffusion, ft^2/s	8.6E-9
Temperature, ˚F	300
One-wing pump rate, bpm	15
Injection time, min	86
Dimensionless horizontal correlation length	0.2
Dimensionless vertical correlation length	0.1
Dimensionless standard deviation of permeability	0.2
Average Young's modulus, MMpsi	8
Effective closure stress, psi	6657

The dimensionless vertical correlation length can be interpreted from variogram shown in **Fig. 3.10**. The vertical correlation length is approximately 23 ft over data range of 232 ft, which gives the dimensionless vertical correlation length approximately 0.1.

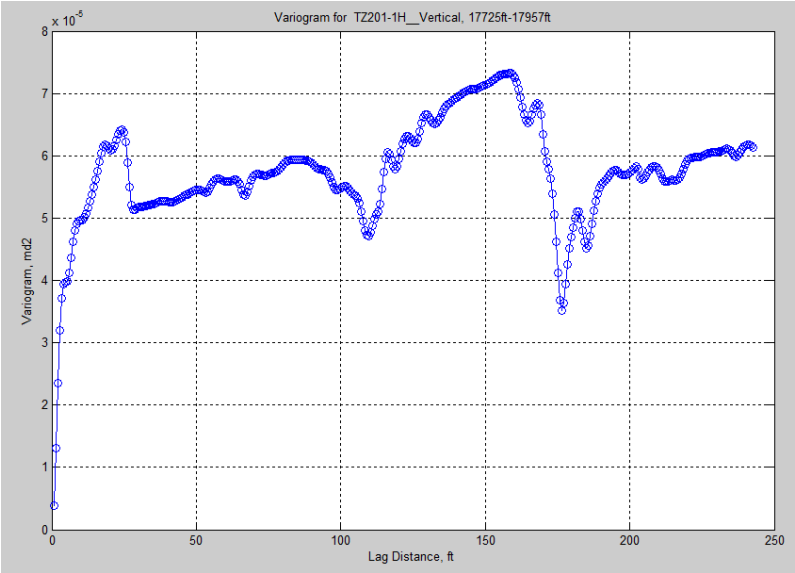

Figure 3.10 – Variogram of Well A vertical permeability distribution within fracture height interval

Since, the permeability distribution along the fracture length direction is difficult to be measured or interpreted, three different values, 0.2, 0.5, and 0.7, were assumed for dimensionless horizontal correlation length for a parametric study. The simulation results of acid fracture conductivities and acid-etched widths are shown in **Fig. 3.11**.

The average acid fracture conductivity based on the simulation results are 30 mD-ft when $\lambda_{D,x}$ equals to 0.2, 50mD-ft when $\lambda_{D,x}$ equals to 0.5, and 60 mD-ft when $\lambda_{D,x}$ equals to 0.7. The corresponding dimensionless fracture conductivities are 36.9, 61.4, and 73.7 using Eq. 1.4.

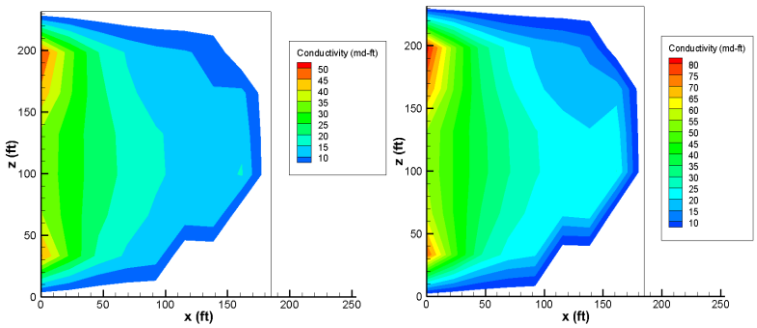

a). Fracture conductivity $\lambda_{D,x}$ =0.2 b). Fracture conductivity $\lambda_{D,x}$ =0.5

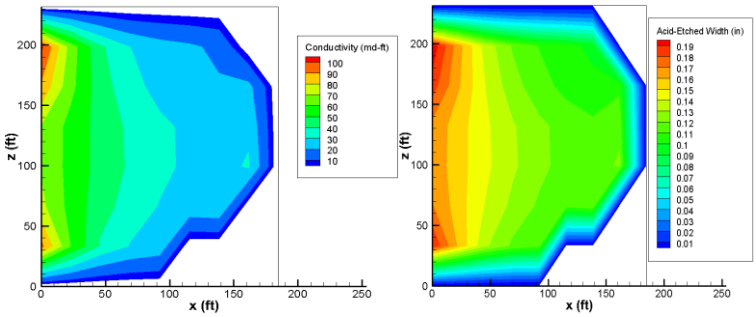

c). Fracture conductivity $\lambda_{D,x}$ =0.7 d). Acid-etched width

Figure 3.11 – Acid fracture conductivity and acid-etched width simulation results

3.5 Post-fracture Production Prediction

The post-treatment production data was provided for the first 113 days after the acid fracturing treatment. The well pressures and the combined gas rate of free gas and gas condensate are shown in **Fig. 3.12**.

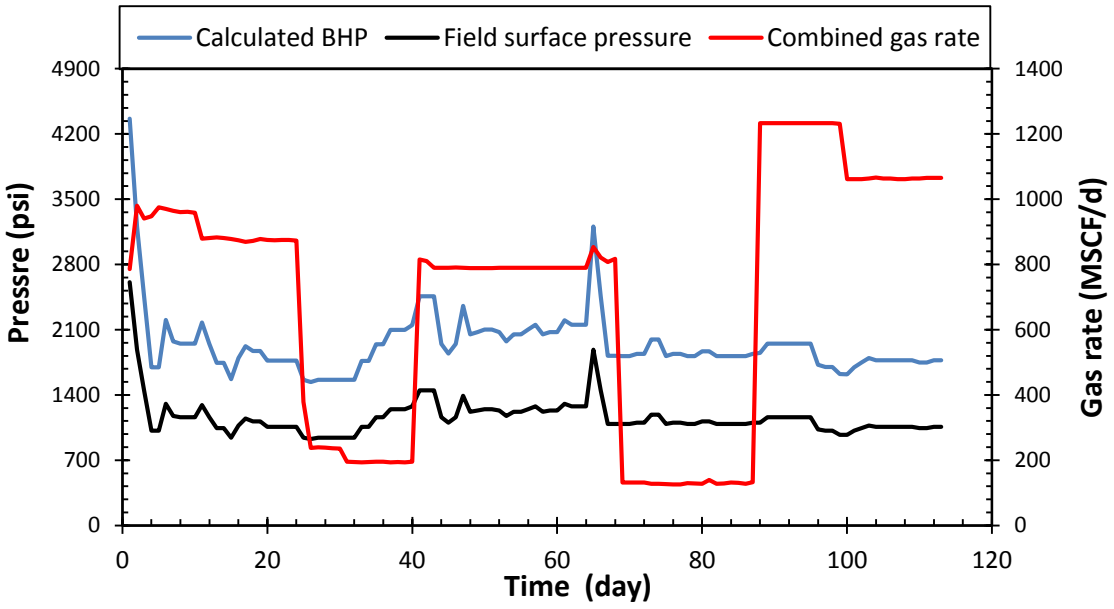

Figure 3.12 – Post-treatment production history

During this production period, the bottomhole flowing pressure is relatively stable with an average value of 2100 psi. The combined gas rate ranges from 180 MSCF/d to 1233 MSCF/d.

To conduct short-term and long-term production predictions for the post-fractured well, the linear flow model by Wattenbarger et al. (1998) is applied. The reservoir and fracture data used for production prediction are shown in **Table 3.8**.

Table 3.8 Reservoir, fracture, and well data for production prediction

Horizontal permeability, mD	0.0044	Initial formation pressure, psi	9985
Vertical permeability, mD	0.000044	$m(p_i)$, psi^2/cp	2.715×10^9
Formation porosity, fraction	0.02	Bottomhole flowing pressure, psi	2100
Formation temperature, ˚F	300	$m(p_{wf})$, psi^2/cp	2.458×10^8
Formation length (b), ft	3000	Distance from the fracture to the	
Formation width, ft	370	formation boundary perpendicular	1500
Formation Thickness, ft	150	to the fracture (y_e), ft	
Gas viscosity, cp	0.035	Fracture half-length, ft	185
Total compressibility, psi^{-1}	5.78E-05	Wellbore radius, ft	0.275
		Initial skin (assumed)	15

The end of transient flow occurs when t_{Dye} is 0.25. From Eq. 2.65, it occurs at 27.2 months.

$$t_{Dye} = \frac{0.0002637kt}{\phi\mu c_t y_e^2} = \frac{0.0002637(0.0044)(t_{months})(30)(24)}{(0.02)(0.035)(5.78\times10^{-5})(1500)^2} = 0.25 \tag{3.6}$$

A 36-month production prediction calculated by Eq. 2.63 – Eq. 2.67 and the actual field production for the first 113 days after the treatment are shown in **Fig. 3.13**. From the figure, the predicted gas production rate has the same order of magnitude of the actual field data.

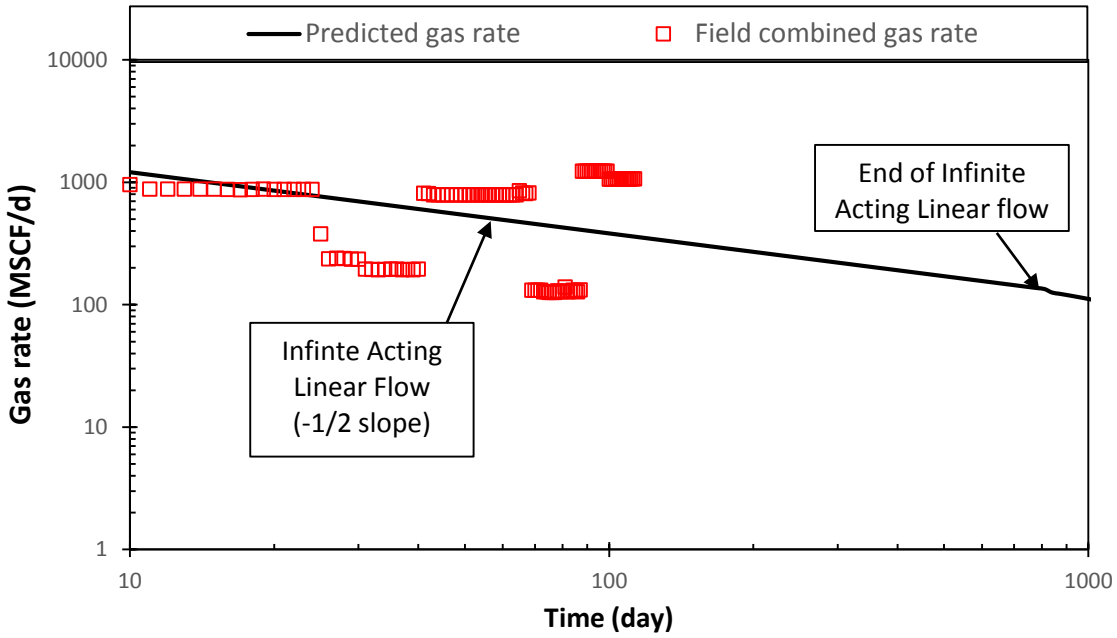

Figure 3.13 – Predicted post-treatment production and actual field production data

For long-term pseudosteady-state condition, the productivity index ratio of the post-treatment to pre-treatment well is calculated by Eq.2.68 – Eq. 2.71,

$$\frac{J_{total}}{J_H} = \frac{\left[\ln\left(\frac{(150\times 370)^{0.5}}{0.275}\right) - 0.259 - 0.75 + 1.074 + 15\right]\times 0.0044\times 150}{\sqrt{0.0044\times 0.000044}\times 3000\times\left(\frac{2}{\pi}\times\frac{1500}{185}\right)} \qquad (3.7)$$

$$= 2.11$$

The results above show productivity index ratio predicted based on the actual field treatment outcomes. Only one fracture was created according to the completion evaluation. It is worthwhile comparing the actual field treatment outcomes with the

designed treatment expectations. It is also worthwhile comparing the multistage acid fracturing treatment with multistage proppant fracturing.

Since the field treatment of Well A has similar operation procedure for each stage, it is assumed that the simulation results of acid fracturing treatment for all six stages are the same. We take stage 1 treatment schedule as the standard. Commercial software MFrac is first run to generate fracture dimensions from fracturing fluids. Then acid fracture conductivity profile is generated using acid fracturing simulator. Productivity index ratio of untreated and post-fractured well is calculated assuming pseudo-steady state condition.

The input for MFrac simulation is the same as in **Table 3.4** except that the pump schedule is now only from stage 1 as shown in **Table 3.2**. The fracture geometry result from MFrac simulation is shown in **Fig. 3.14**. The fracture has a fracture half-length of 155 ft, a fracture height of 92 ft, and the maximum fracture width is about 0.1 inches. It is observed that since less fracturing fluid was used, the fracture are shorter and more contained than the fracture in the previous case.

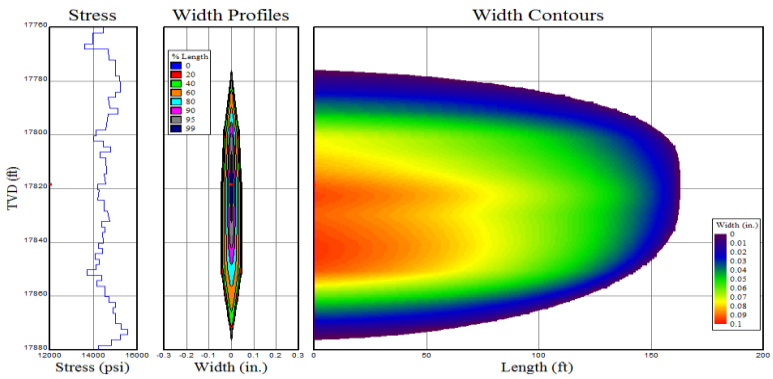

Figure 3.14 – Fracture geometry with for stage 1 treatment.

For acid fracturing simulation, assuming all acids from stage 1 treatment design are injected into the fracture after fracture is initiated, the total acid injection time is now adjusted to 50 minutes with an average total injection rate 30 bpm. The new acid fracturing simulation input data is shown in **Table 3.9**.

Table 3.9 Input parameters for acid fracturing simulator

Newtonian viscosity, cp	30
Fluid density, lb/ft^3	68.6
Formation porosity, fraction	0.02
Acid concentration, wt%	20
Effective diffusion, ft^2/s	8.6E-9
Temperature, ˚F	300
One-wing pump rate, bpm	15
Injection time, min	50
Dimensionless horizontal correlation length	0.2
Dimensionless vertical correlation length	0.1
Dimensionless standard deviation of permeability	0.2
Average Young's modulus, MMpsi	8
Effective closure stress, psi	6657

Three different dimensionless horizontal correlation lengths 0.2, 0.5, and 0.7 were tested and the results are shown in **Fig. 3.15**. In **Fig. 3.15**, picture a shows that the final acid fracture conductivity is 24 mD-ft when $\lambda_{D,x}$ equals to 0.2, picture b shows that the

final acid fracture conductivity is 36 mD-ft when $\lambda_{D,x}$ equals to 0.5, and picture c shows that the final acid fracture conductivity is 42 mD-ft when $\lambda_{D,x}$ equals to 0.7.

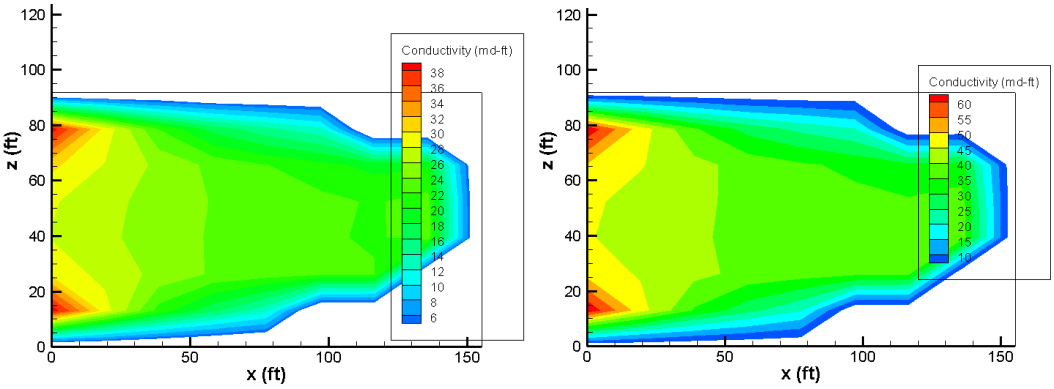

a) Fracture conductivity $\lambda_{D,x}$ =0.2

b) Fracture conductivity $\lambda_{D,x}$ =0.5

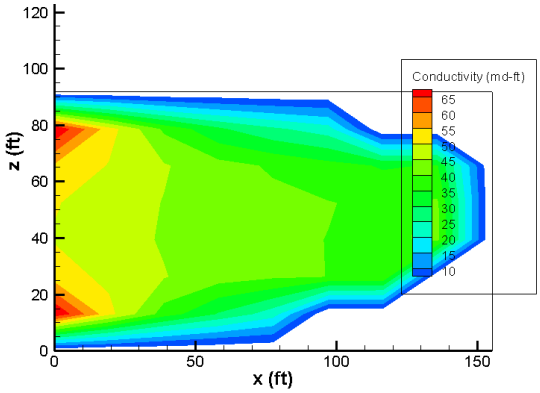

c) Fracture conductivity $\lambda_{D,x}$ =0.7

Figure 3.15 – Acid fracture conductivity simulation results for stage 1 treatment

The corresponding dimensionless fracture conductivities C_{fD} defined by Eq. 1.4 are 35 when $\lambda_{D,x}$ equals to 0.2, 53 when $\lambda_{D,x}$ equals to 0.5, and 62 when $\lambda_{D,x}$ equals to 0.7. The

equivalent skin factor then can be calculated using Eq. 1.5 which ranges from -5.60 to -5.62. For this case, we take an average equivalent skin factor of -5.61.

Assume same reservoir properties as shown in **Table 3.8** are used to predict post-treatment productivity index. The total drainage area is now divided into six rectangular blocks with 500 ft length and 370 ft width. The equivalent drainage radius is 292 ft if use Dietz shape factor of 21.8 for an aspect ratio of 1:2; and 245 ft if use Dietz shape factor of 30.9 for an aspect ratio of 1:1. We take an average equivalent drainage radius of 267 ft for productivity index calculation.

Assume initial skin factor is negligible, the productivity index ratio can be determined by,

$$\frac{J_{total}}{J_H} = \frac{\left[\ln\left(\frac{(150\times 370)^{0.5}}{0.275}\right) - 0.259 - 0.75 + 1.074\right]\times 6\times 0.0044\times 92}{\sqrt{0.0044\times 0.000044}\times 3000\times\left(\ln\left(\frac{267}{0.275}\right) - 0.75 - 5.61\right)} \quad (3.8)$$

$$= 23$$

From the calculation, if the 6-stage acid fracturing treatment were performed as designed, a 23-fold increase in productivity can result from the treatment.

Due to difficulties in acid fracturing treatment design, such as uncertainties in fracture conductivity prediction due to formation heterogeneity and controlling the depth of acid penetration, proppant fracturing treatment is often performed in carbonate formation. In this study, a 6-stage proppant fracturing treatment is also simulated in order to compare with the simulation results of acid fracturing.

In propped fracture simulation, the goal is to create a fracture that has a significantly longer effective fracture half-length and more contained fracture height compares to acid fracturing. For this field case, a constant bottomhole flowing pressure of 2100 psi can lead to a high effective closure pressure as 12455 psi. Two types of proppant, a 20/40 mesh proppant and a 40/70 mesh proppant, are tested for different fracture conductivity the treatment can achieve. Treatment schedule and input data for both cases are shown in **Table 3.10**.

Table 3.10 Proppant fracturing treatment simulation data

20/40 mesh proppant		40/70 mesh proppant	
Total fluid volume/ stage, gal	54,335	Total fluid volume/ stage, gal	54,335
Pad fluid percentage	40%	Pad fluid percentage	40%
Average pump rate, bpm	30	Average pump rate, bpm	30
Total proppant mass, lbm	11,012	Total proppant mass, lb	11,012
Proppant diameter, in	0.0287	Proppant diameter, in	0.0118
Expected conductivity at 12,000 effective closure stress with 0.5 lbm/ft^2 concentration, mD-ft	158	Expected conductivity at 12,000 effective closure stress with 0.5 lbm/ft^2 concentration, mD-ft	82

MFrac is used for proppant fracturing treatment simulation. For 20/40 mesh proppant fracturing, the results are shown in **Fig. 3.16**. For 40/70 mesh proppant fracturing, the results are shown in **Fig. 3.17**. From the simulation results, the effective fracture half-length using 40/70 proppant is 230 ft, propped fracture height is 150 ft, and

average fracture conductivity is 56 mD-ft. While using 40/70 mesh proppant, the effective fracture half-length is 265 ft, the propped fracture height is 190 ft, and average fracture conductivity is 25 mD-ft.

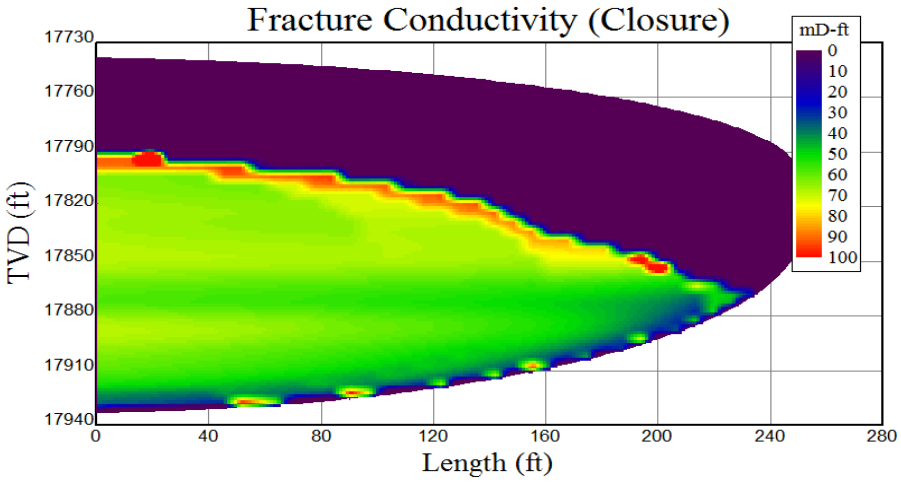

Figure 3.16 – Fracture conductivity at the end of treatment using 20/40 proppant

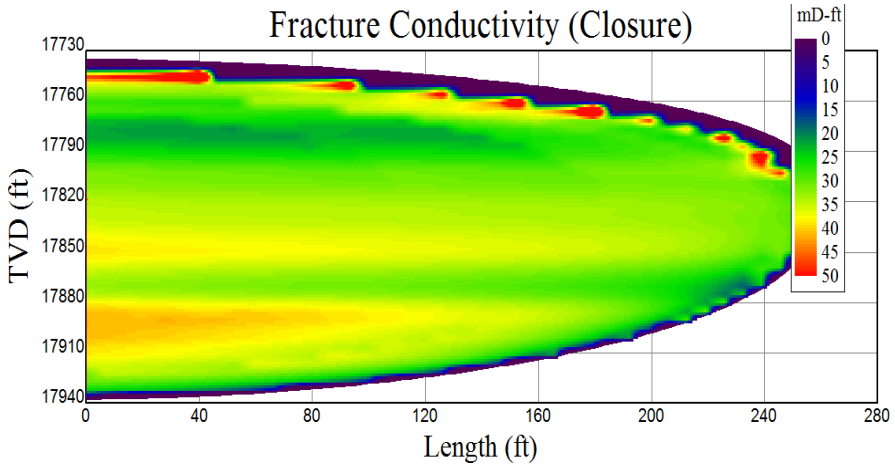

Figure 3.17 – Fracture conductivity at the end of treatment using 40/70 proppant

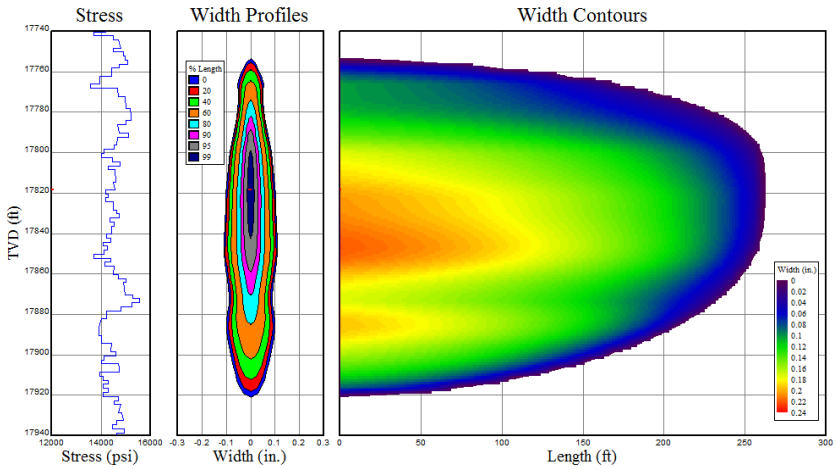

Figure 3.18 – Fracture width profile at the end of treatment

For productivity calculation, it is assumed that for propped fracture, since longer fracture can contact with further hydrocarbon reserves, the width of reservoir drainage area extended to 700 ft instead of 370 ft. The equivalent drainage radius is 402 ft if assume Dietz shape factor of 21.8 for aspect ratio of 1:2, and 337 ft if assume Dietz shape factor of 30.9 for aspect ratio of 1:1, thus we take an average of equivalent drainage radius of 370 ft for productivity prediction.

Eq. 1.5 is used to calculate equivalent skin factor. For 40/70 mesh proppant case, the equivalent skin is -6.1, and for 20/40 mesh proppant case, the equivalent skin is -6. The productivity index ratio then can be calculated, assume all six stages have the same simulation results, and other properties are the same as shown in **Table 3.8**. For 20/40 mesh proppant case,

$$\frac{J_{total}}{J_H} = \frac{\left[\ln\left(\frac{(150\times 700)^{0.5}}{0.275}\right) - 0.463 - 0.75 + 1.074\right]\times 6\times 0.0044\times 150}{\sqrt{0.0044\times 0.000044}\times 3000\times\left(\ln\left(\frac{370}{0.275}\right) - 0.75 - 6\right)} \quad (3.4)$$

$$= 47$$

for 40/70 mesh proppant case,

$$\frac{J_{total}}{J_H} = \frac{\left[\ln\left(\frac{(150\times 700)^{0.5}}{0.275}\right) - 0.463 - 0.75 + 1.074\right]\times 6\times 0.0044\times 150}{\sqrt{0.0044\times 0.000044}\times 3000\times\left(\ln\left(\frac{370}{0.275}\right) - 0.75 - 6.1\right)} \quad (3.4)$$

$$= 60$$

From the calculation, a 6-stage proppant fracturing treatment can achieve 47-fold productivity increase using 20/40 mesh proppant. If use a smaller proppant size 40/70, 60-fold productivity increase can be achieved due to longer effective fracture half-length.

3.6 Results and Discussion

From the treatment evaluation using the integrated evaluation approach, it is concluded that Well A multi-stage acid fracturing treatment created one fracture at stage 1. The fracture dimension is approximately 185 ft for fracture half-length, 231 ft for fracture height. The average acid fracture conductivity ranges between 30 mD-ft and 60 mD-ft. The cumulative gas production predicted at 36 months after the treatment is approximately 225 MMSCF under a constant bottomhole flowing pressure of 2100 psi. The productivity-index ratio shows a 2.11-fold productivity increase for the post-fractured well.

If the 6-stage acid fracturing is carried out as designed, the simulation results show a fracture with fracture half-length of 155 ft, fracture height of 92 ft, and an average fracture conductivity ranges from 24 mD-ft to 54 mD-ft can be achieved for each stage. Post-fractured well can achieve 75 times higher productivity compares to untreated well.

6-stage proppant fracturing treatment is also simulated to compare with acid fracturing treatment results. Two types of proppant are tested. Using 20/40 mesh proppant, an effective fracture half-length of 230 ft, propped fracture height of 150 ft, and an average fracture conductivity of 60 mD-ft can be achieved for each stage. This will give a 47-fold increase in productivity compared to untreated well. If 40/70 mesh proppant is used, an effective fracture half-length of 265 ft, propped fracture height of 190 ft, and an average fracture conductivity of 25 mD-ft can be achieved for each stage. This will give a 60-fold increase in productivity compared to untreated well.

From the completion evaluation results, the pressure-controlled sliding sleeves with open-hole packers were not functioning in isolating stages in this particular treatment. The failure in activating pressure-controlled sleeves is mainly due to the low seating efficiency of ball sealers. Numerous papers have been published on the ball sealer seating efficiency in a vertical well, but not many for ball sealer behavior in a horizontal well because the force balance is complicated by perforation facing, perforation spacing, use of non-buoyant or buoyant ball sealers, and the wall effect. A thorough study on ball sealer behavior in a horizontal pipe will be helpful for improving the performance of ball sealers in a horizontal well multi-stage treatment.

Through the study of this field case, it is noticed that an accurate bottomhole pressure, either measured from downhole pressure gauge or calculated from surface pressure, is critical in evaluating a multi-stage treatment. It is the key to link the well completion evaluation and the fracture modeling. The difficulties in obtaining an accurate bottomhole pressure in this field application are mainly caused by 1) there is no downhole pressure gauge installed; 2) the treating fluids' rheology provided are incomplete. Only the density and an apparent viscosity were given for each treating fluid. Large error may occur when interpreting fluid tubing frictions from the surface treating pressures for a non-Newtonian fluid due to its varying viscosity with respect to the fluid velocity and tubing size. Especially in this field case, the available measurements for crosslinked acid were limited, therefore, the bottomhole pressure calculated during the crosslinked acid injection may not represent the exact bottomhole pressure during the fracturing treatment.

In this field case, no pre-fracture diagnostic tests had been conducted. The formation closure stress is solely based well log interpretation. A step-rate test is strongly recommended for identifying the formation closure stress. Accurate stress profiles are very crucial in fracturing treatment design, especially in a heterogeneous carbonate formation.

A more accurate production prediction can be performed by using reservoir simulations if detailed geological information are provided. The acid fracture dimensions and conductivity can be coupled with the reservoir grids. However, in this case, the production prediction using linear flow model shows a good match with actual field measurement. Therefore, with limited information on the reservoir properties, the final

results of the well performance predicted from the integrated evaluation approach is acceptable.

The proppant fracturing simulation results show better post-fractured well performance comparing to acid fracturing. The conductivity of the acid fracture is created by the unevenly etched fracture surface due to acid/rock reaction, from the acid fracture conductivity correlations, it is clear that higher the closure stress, lower the fracture conductivity. Therefore for deep carbonate formations with high closure stress, the acid fracture conductivity may reduce significantly once production starts, which leads to poor treatment performance. On the other hand, for low permeability reservoirs, it is critical to create fractures that have sufficiently long effective fracture half-length to make the largest contact with the reservoir. However, currently it is difficult to design acid fracturing treatment to achieve this goal due to limited acid etched penetration by high fluid loss and temperature effect. For this field case study, we conclude that multistage proppant fracturing is a more reliable stimulation method for Well A in deep carbonate formation with low permeability and high closure stress.

CHAPTER IV

CONCLUSION

In this research, an integrated approach for evaluating a horizontal well multi-stage acid fracturing treatment is developed. A field example is used to demonstrate the application of the developed approach. The integrated approach is proven to be successful in simulating the treatment outcomes and predicting post-stimulation well performance. This approach consists of three parts, 1) completion evaluation, 2) acid fracturing simulation, and 3) post-fractured well performance prediction. This integrated approach can analyze stage isolation in different well completions for multi-stage treatments including ball-activated sliding sleeves with open-hole packers, ball sealer in cased and perforated wells, and pressure-controlled sliding sleeves with open-hole packers. In this approach, fracture geometry is simulated by commercial software. According to the requirements of model accuracy and computational time, the PNK model, the KGD model, or a pseudo-3D fracture propagation model can be selected. The final acid fracture conductivity profile is generated by a fully 3D acid fracturing simulator. The integrated treatment evaluation approach will provide a post-treatment well performance prediction using a productivity model that fits the field conditions. Comparing simulation results from multistage acid fracturing treatment and proppant fracturing treatment of this field case, it is observed that for low permeability carbonate formation with high closure stress, multistage proppant fracturing can achieve higher productivity index ratio. When design

a treatment for a well in carbonate formation, it is worthwhile to investigate all possible stimulation methods to determine the optimal one for the well.

Future work can focus on improving model efficiency in current approach. Even though the evaluation approach is comprehensive, each section in this approach is evaluated or modeled separately. Any change of outcomes from one section need to be manually updated to the next section. By developing a fully couple acid fracturing simulator, which can model fracture propagation and acid transport and reaction processes simultaneously, this integrated evaluation approach will be more accurate and effective when modeling acid fracturing treatment with multi-stage fluid systems.

REFERENCES

Angeles, R., Tolman, R., Gupta, J., Benish, T., Ross, K., Cole, S., and Lopez, T. 2012. One Year of Just-In-Time Perforating as Multi-Stage Fracturing Technique for Horizontal Wells. SPE 160034. Presented at the SPE Annual Technical Conference and Exhibition, San Antonio, TX, 8-10 October.

Augustine, J., and Meijs, R. 2011. Modeling the Dynamic Pressure Response of Ball-Actuated Stimulation Sleeves. *SPE Production & Operations*, 26(02): 162-172.

Babaniyazov, A., and Jackson, C.H. 2013. Methodological Approach for Optimization of Completion Practices in Mature Carbonate Fields. SPE 166249. Presented at the SPE Annual Fall Technical Conference and Exhibition, New Orleans, LA, 30 September – 2 October.

Babu, D.K., and Odeh, A.S. 1989. Productivity of a Horizontal Well. *SPE Reservoir Engineering* 4(04): 417-412.

Babu, D.K., and Odeh, A.S. 1988. Productivity of a Horizontal Well. SPE 18334. Presented at the SPE Annual Technical Conference and Exhibition, Houston, TX, 2-5 October.

Barker, B.J. and Ramey, H.J., Jr. 1978. Transient Flow to Finite Conductivity Vertical Fractures. SPE 7489. Presented at the SPE Annual Fall Technical Conference and Exhibition, Houston, TX, 1-3 October.

Barnea, E. and Mizrahi, J. 1973. A Generalized Approach to the Fluid Dynamics of Particle Systems: Part 1. General Correlation for Fluidization and Sedimentation in Solid Multiparticle Systems. *The Chemical Engineering Journal* 5(2): 171-189.

Baumgarten, D., and Bobrosky, D. 2009. Multi-Stage Acid Stimulation Improves Production Values in Carbonate Formations in Western Canada. SPE 126058. Presented at the SPE Saudi Arabia Section Technical Symposium, Al-Khobar, Saudi Arabia, 9-11 May.

Bern, P.A. and Lewis, R.C. 1992. Ball Sealer Diversion in Deviated Wellbores. Interim report, BP, Sunbury-on-Thames, United Kingdom (unpublished).

Biot, M.A. and Willis, D.G. 1957. The Elastic Coefficient of the Theory of Consolidation. *Journal of Applied Mechanic*: 594-618.

Brown, R.W., Neill, G.H., and Loper, R.G. 1963. Factors Influencing Optimum Ball Sealer Performance. *JPT* 15(04): 450-454.

Chen, N.H. 1979. An Explicit Equation for Friction Factor in Pipe. *Ind. Eng. Chem. Fund*. 18(296).

Carter, R.D. 1957. Appendix to Optimum Fluid Characteristics for Fracture Extension, by Howard, G.C., and Fast, C.R. *Drill. and Production Prac., API* 24: 261-270.

Casero, A., Adefashe, H., and Phelan, K. 2013. Open Hole Multi-Stage Completion System in Unconventional Plays: Efficiency, Effectiveness and Economics. SPE paper 164009. Presented at the SPE Middle East Unconventional Gas Conference and Exhibition, Muscal, Oman, 28-30 January.

Chhabra, R.P., Agarwal, S., and Chaudhary, K. 2003. A Note on Wall Effect on the Terminal Falling Velocity of a Sphere in Quiescent Newtonian Media in Cylindrical Tubes. *Powder Technology* 129 (1-3): 53-58.

Cinco-Ley, H. and Samaniego-V., F. 1981. Transient Pressure Analysis for Fractured Wells. *JPT* 33(09): 1749-1766.

Deng, J., Mou, J., Hill, A.D., and Zhu, D. 2011. A New Correlation of Acid-Fracture Conductivity Subject to Closure Stress. SPE 140402. Presented at the SPE Hydraulic Fracturing Technology Conference and Exhibition, The Woodlands, TX, 24-26 January.

Erbstoesser, S.R. 1980. Improved Ball Sealer Diversion. *JPT* 32 (11): 1903-1910.

Etuhoko, M., Viti, M., Akutin, A. Zmeyevskiy, S., and Caproni, C. 2014. Openhole Multistage Fracture Completion with Swelling Packers and Sliding Sleeves in Carbonate Reservoir – A Case History from the Karachaganak Field. SPE 172340. Presented at the SPE Annual Caspian Technical Conference and Exhibition, Astana, Kazakhstan, 12-14 November.

Gabriel, G.A. and Erbstoesser, S.R. 1984. The Design of Buoyant Ball Sealer Treatments. SPE 13085. Presented at the SPE Annual Technical Conference and Exhibition. Houston, TX, 16-19 September.

Geertsma, J., and de Klerk, F.A. 1969. Rapid Method of Predicting Width and Extent of Hydraulically Induced Fractures. *JPT*, 21(12): 1571-1581.

Kalfayan, L.J. 2007. Fracture Acidizing: History, Present State, and Future. SPE 106371. Presented at the SPE Hydraulic Fracturing Technology Conference, College Station, TX, 29-31 January.

Li, X., Chen, Z., Chaudhary, S.A. et al. 2005. An Integrated Transport Model for Ball-Sealer Diversion in Vertical and Horizontal Wells. SPE 96339. Presented at the SPE Annual Technical Conference and Exhibition, Dallas, TX, 9-12 October.

Lo, K.K. and Dean, R.H. 1989. Modeling of Acid Fracturing. *SPE Prod. Eng.* 4(02): 194-200.

Metcalf, A.S., Miller, H.L., Weaver, R.T., Swain, M.L., Nordstog, K., and Fallon, J. 2007. Case History: Acid Fracturing Deep Hot Ellenburger. SPE 106986. Presented at the SPE Production and Operations Symposium, Oklahoma City, OK, 31 March – 3 April.

Meyer, B.R. 1986. Design Formulae for 2-D and 3-D Vertical Hydraulic Fractures: Model Comparison and Parametric Studies. SPE 15240. Presented at the SPE Unconventional Gas Technology Symposium, Louisville, KY, 18-21 May.

Meyer, B.R. 1989. Three-Dimensional Hydraulic Fracturing Simulation on Personal Computers: Theory and Comparison Studies. SPE 19329. Presented at the SPE Eastern Regional Meeting, Morgantown, WV. 24-27 October.

Meyer, B.R. 1990. Real-Time 3-D Hydraulic Fracturing Simulation: Theory and Field Case Studies. SPE 20658. Presented at the SPE Annual Technical Conference and Exhibition, New Orleans, LA, 23-26 September.

Meyer, B.R., Jacot, R.H. 2005. Pseudosteady-State Analysis of Finite Conductivity Vertical Fractures. Paper SPE 95941 presented at the SPE Annual Technical Conference and Exhibition, Dallas, TX, 9-12 October.

Morales, R.H., and Sayed, A.S.1989. Microcomputer Analysis of Hydraulic Fracture Behavior with a Pseudo-Three-Dimensional Simulator. *SPE Production Engineering*, 4(01): 69-74.

Ming, G., Lacote, S., Hill, A.D. 1999. New Model of Acid-Fracture Conductivity Based on Deformation of Surface Asperities. *SPEJ*, 4(03): 206-214.

Mou, J., Hill, A.D., Zhu, D. 2007. The Velocity Field and Pressure Drop Behavior in a Rough-Walled Fracture. SPE 105182. Presented at the SPE Hydraulic Fracturing Technology, College Station, TX, 29-31 January.

Mou, J., Hill, A.D., Zhu, D. 2009. Acid-Etched Channels in Heterogeneous Carbonates-A newly Discovered Mechanism for Creating Acid Fracture Conductivity. SPE 119619. Presented at the SPE Hydraulic Fracturing Technology Conference, The Woodlands, TX, 19-21 January.

Nainwal, S.P., Agarwal, P., Haldar, S. 2006. Multistage Controlled Acid Fracturing: A Unique Acid-Stimulation System Proved Efficient in a Field of Bombay Offshore Basin

– A Case Study. SPE 101243. Presented at the SPE International Oil & Gas Conference and Exhibition, Beijing, China, 5-7 December.

Neill, G.H., Brown, R.W., and Simmons, C.M. 1957. An Inexpensive Method of Multiple Fracturing. *Drilling and Production Practice*: 27-32.

Nierode, D.E., and Kruk, K.F. 1973. An Evaluation of Acid Fluid Loss Additives, Retarded Acids, and Acidized Fracture Conductivity. Paper SPE 39776. Presented at the SPE Permian Basin Oil and Gas Recovery Conference, Midland, TX, 23-26 March.

Nieto, C. M., Pournik, M., & Hill, A. D. 2008. The Texture of Acidized Fracture Surfaces: Implications for Acid Fracture Conductivity. *SPE Prod. & Oper.* 23(03): 343-352.

Nordgren, R.P. 1972. Propagation of a Vertical Hydraulic Fracture. *SPEJ*, 12(04): 306-314.

Nozaki, M., Zhu, D., Hill, A.D. 2013. Experimental and Field Data Analyses of Ball-Sealer Diversion. *SPE Prod. & Oper*, 28(03): 286-295.

Oeth, C.V., Hill, A.D., and Zhu, D. 2013. Acid Fracturing: Fully 3D Simulation and Performance Prediction. SPE 163840. Presented at the SPE Hydraulic Fracturing Technology Conference, The Woodlands, TX, 4-6 February.

Palmer, I.D., Carroll, H.B. 1983. Three-Dimensional Hydraulic Fracture Propagation in the Presence of Stress Variations. *SPEJ*. 23(06): 870-878.

Perkins, T.K., and Kern, L.R. 1961. Widths of Hydraulic Fractures. *JPT*, 13(09): 937-949.

Romero, J., Gu, H., and Gulrajani, S.N. 2001. 3D Transport in Acid-Fracturing Treatments: Theoretical Development and Consequences for Hydrocarbon Production. *SPE Prod. & Fac.* 16(2): 122-130.

Prats, M. 1961. Effect of Vertical Fractures on Reservoir Behavior-Incompressible Fluid Case. *SPEJ*, 1(02): 105-118.

Seale, R., Themig, D., Athans, J. 2006. Effective Stimulation of Horizontal Wells – A New Completion Method. SPE 106357. Presented at the SPE Technical Symposium of Saudi Arabia, Dhahran, Saudi Arabia, 21-23 May.

Seale, R. 2007. An Efficient Horizontal Openhole Multistage Fracturing and Completion System. SPE 108712. Presented at the SPE International Oil Conference and Exhibition, Veracruz, Mexico, 27-30 June.

Settari, A., and Cleary, M. 1986. Development and Testing of a Pesudo-Three-Dimensional Model of Hydraulic Fracture Geometry. *SPE Production Engineering*, 1(06): 449-466.

Settari, A. 1993. Modeling of Acid-Fracturing Treatments. *SPE Prod. & Fac*, 8(1): 30-38.

Simonson, E.R., Abou-Sayed, A.S., and Clifton, R.J. 1978. Containment of Massive Hydraulic Fractures. *SPEJ*, 18(01): 27-32.

Song, B., Economides, M.J., Ehlig-Economides, C.A. 2011. Design of Multiple Transverse Fracture Horizontal Wells in Shale Gas Reservoirs. SPE 140555. Presented at the SPE Hydraulic Fracturing Technology Conference, The Woodlands, TX, 24-26 January.

Tada, H., Paris, P., and Irwin, G. 1973. *The Stress Analysis of Crack Handbook*. Del Research Corp. Hellertown, PA.

Tompkins, R., Smith, N., Wellhoefer, B., Yuyi, S., Rhodes, B., and Stivers, P. 2013. Factors Affecting Effective Millout of Multistage Fracturing Sleeves in Horizontal Wellbores. SPE 163899. Presented at the SPE/ICoTA Coiled Tubing & Well Intervention Conference & Exhibition, The Woodlands, TX, 26-27 March.

Wattenbarger, R.A., El-Banbi, A.H., and Villegas, M.E. 1998. Production Analysis of Linear Flow into Fractured Tight Gas Wells. SPE 39931. Presented at the SPE Rocky Mountain Regional Low Permeability Reservoir Symposium and Exhibition, Denver, CO, 5-8 April.

Weng, X. 1992. Incorporation of 2D Fluid Flow into a Pseudo-3D Hydraulic Fracturing Simulator. *SPE Production Engineering*, 7(04): 331-337.

White, F.M. 1986. *Fluid Mechanics*. New York: McGraw-Hill Book Co.

Zheltov, Y.P., and Khristianovitch, S.A. 1955. On the Mechanism of Hydraulic Fracturing of an Oil-Bearing Stratum. *OTN*, 5: 3-41.